Lithos 134–135 (2012) 236–252

Contents lists available at SciVerse ScienceDirect

Lithos

journal homepage: www.elsevier.com/locate/lithos

Geochronology and petrogenesis of gray gneisses from the Taihua Complex at Xiong'er in the southern segment of the Trans-North China Orogen: Implications for tectonic transformation in the Early Paleoproterozoic

Xiao-Long Huang [a,b,*], Simon A. Wilde [b], Qi-Jun Yang [a,c], Jun-Wei Zhong [a,d]

[a] State Key Laboratory of Isotope Geochemistry, Guangzhou Institute of Geochemistry, Chinese Academy of Sciences, Guangzhou 510640, China
[b] Department of Applied Geology, Curtin University of Technology, PO Box U1987, Perth, Western Australia 6845, Australia
[c] College of Earth Sciences, Guilin University of Technology, Guilin 541004, China
[d] Graduate University of Chinese Academy of Sciences, Beijing 100049, China

ARTICLE INFO

Article history:
Received 1 November 2011
Accepted 8 January 2012
Available online 14 January 2012

Keywords:
Potassium-rich igneous rocks
Thickened crust
Post-collisional magmatism
TTG gneisses
Taihua Complex
Trans-North China Orogen

ABSTRACT

The Taihua Complex in the Xiong'er area along the southern segment of the Trans-North China Orogen (TNCO) consists of gray gneisses with minor amphibolites. Zircon U–Pb dating of the gray gneisses reveals at least two episodes of Early Paleoproterozoic magmatism (2.30–2.32 Ga and 2.07–2.19 Ga), each with distinct geochemical features. The Tieluping TTG gneisses of the early suite have very low HREE ($Yb_N = 0.58 - 4.75$) and Y contents (2.05–13.2 ppm) with moderate to high $[La/Yb]_N$ (14.3–192.6) and Sr/Y ratios (38.5–220.1), pronounced negative Ta–Nb and Ti anomalies but positive Sr and Pb anomalies. The protoliths of these gneisses were most likely derived from partial melting of thickened lower crust with residual garnet and amphibole, and underwent garnet ± amphibole fractionation, plagioclase accumulation and/or fractionation. The Tieluping TTG gneisses have variable zircon Hf model ages ($T^C_{DM\text{-}Hf} = 2.48 - 3.06$ Ga) and whole-rock $\varepsilon_{Nd}(t)$ values (−4.89–4.98), and the youngest whole-rock depleted mantle Nd model age ($T_{DM} = 2.32$ Ga) is close to the crystallization age of the TTG (2318 ± 8 Ma). The protolith of the gneisses formed from a combination of pre-existing continental crust and juvenile materials, implying an Andean-type continental margin arc environment. It is suggested that crustal thickening was the result of accretionary orogenesis accompanied by basaltic underplating. The Ganshugou potassium-rich gneisses of the later suite have low Na_2O and high K_2O, and show fractionated LREE and nearly flat HREE patterns, with strong negative Ta-Nb and Ti anomalies. They are characterized by negative $\varepsilon_{Nd}(t)$ values (−5.01 to −2.33) and heterogeneous zircon $\varepsilon_{Hf}(t)$ values (−10.65–2.10) with decoupling of zircon Hf model ages ($T^C_{DM\text{-}Hf} = 2.64 - 3.23$ Ga) and whole-rock Nd model ages ($T_{DM} = 2.55 - 2.81$ Ga). The protolith of the Ganshugou gneisses was a potassium-rich igneous rock, which was likely the result of partial melting of pre-existing crustal materials at shallow depth, compatible with a post-collisional setting. There is therefore a tectonic transformation from an accretionary orogenesis to an extensional regime as a consequence of post-collisional uplift in the southern segment of the TNCO in the Early Paleoproterozoic.

1. Introduction

The global episodic peaks of crustal formation (2.7 Ga, 1.9 Ga and 1.2 Ga; Condie, 2000; Kemp et al., 2006) suggest there may have been a widespread reduction in magmatic activity on Earth in the period between 2.45 and 2.20 Ga, which might be a globally significant period of cessation or slowdown of plate tectonics (Condie et al., 2009). However, the North China Craton (NCC) is unusual in this regard for it contains abundant evidence for magmatic and tectonic activities in the Trans-North China Orogen (TNCO) (Fig. 1a) during this period (e.g., Zhao et al., 2008). The TNCO may contain one of the longest-lived magmatic arcs (>650 Ma; Zhao et al., 2008).

The Taihua "group" is a traditional term for the Late Archean to Early Paleoproterozoic metamorphic complex exposed along the southern segment of the TNCO (Fig. 1a). Although the Taihua Complex is commonly considered to be the most important Early Precambrian unit in the southern part of the TNCO, Early Paleoproterozoic magmatism appears to be rare. The question is whether this can be attributed to insufficient geochronological studies or whether it is real. In the Lushan area, the Taihua Complex reveals the Neoarchean crustal transition from ocean crust formation to subducting-slab melting, and intracrustal reworking (Huang et al., 2010). In the Xiong'er area, the Taihua Complex is generally comparable to that at Lushan, and

* Corresponding author at: Guangzhou Institute of Geochemistry, Chinese Academy of Sciences, P.O. Box 1131, Guangzhou 510640, China. Tel.: +86 20 85290010; fax: +86 20 85291510.
E-mail address: xlhuang@gig.ac.cn (X.-L. Huang).

0024-4937/$ – see front matter © 2012 Elsevier B.V. All rights reserved.
doi:10.1016/j.lithos.2012.01.004

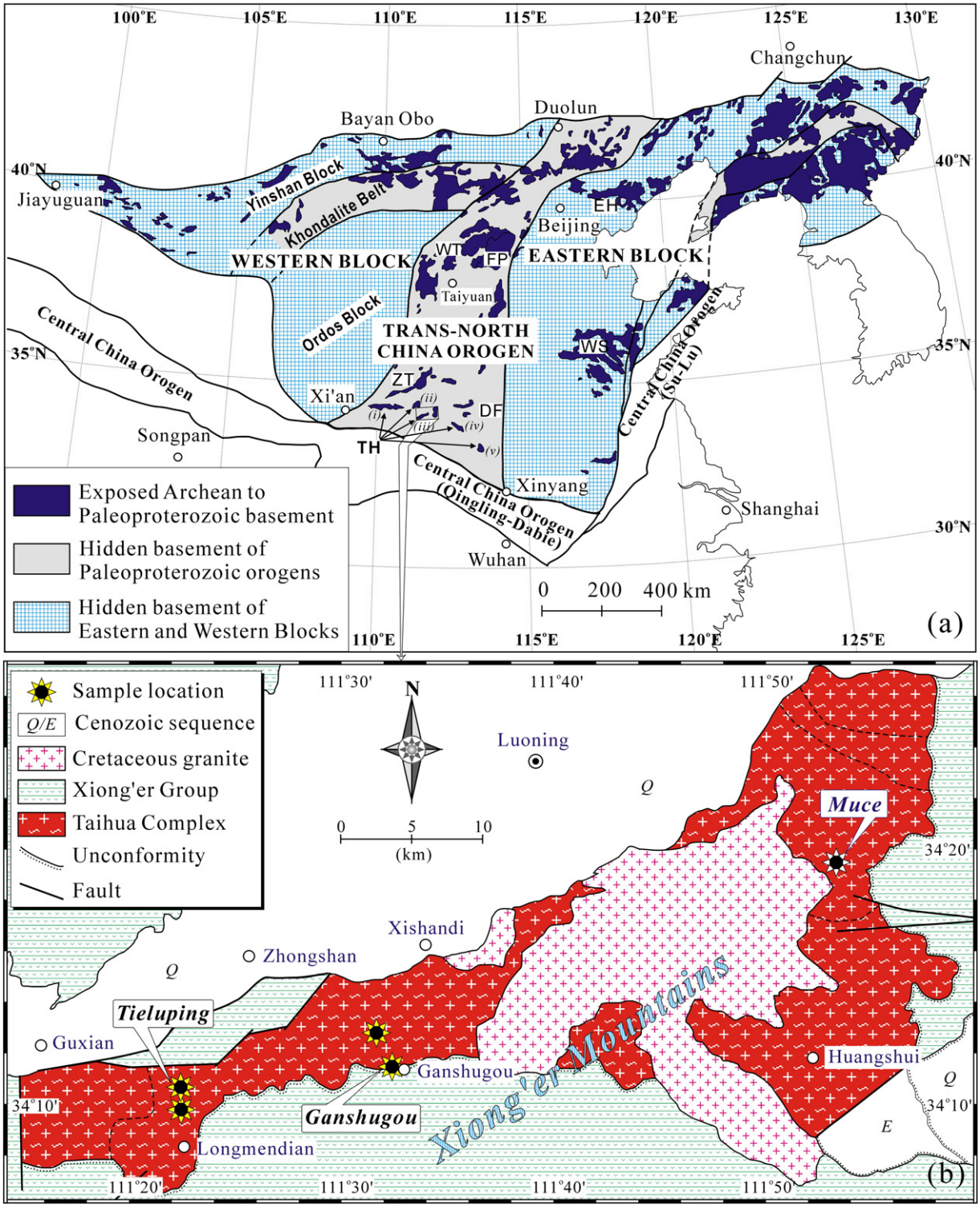

Fig. 1. (a) Tectonic framework of the North China Craton (NCC) showing the Eastern Block, Western Block, Trans-North China Orogen and exposed Archean to Paleoproterozoic basement (after Zhao et al., 2005); the Taihua "group" (TH) and the Dengfeng "group" (DF) metamorphic complexes are distributed at the southern margin of the NCC. The Taihua "group" includes: (i) Xiaoqinling; (ii) Xiaoshan; (iii) Xiong'er Mountain; (iv) Lushan; and (v) Wuyang. Abbreviations of other metamorphic complexes: Zhongtiaoshan (ZT), Wutaishan (WT), Fupin (FP), Western Shandong (WS), Eastern Hebei (EH); (b) geological map of the Xiong'er Mountains region, illustrating the distribution of the Taihua Complex, the Xiong'er group and sample locations; Modified from the Luoning geological map at 1:200,000 scale (BGMR (Bureau of Geology and Mineral Resources), 1965).

is also considered to have formed during the Late Neoarchean and undergone metamorphism in the Paleoproterozoic, mostly based on Sm–Nd isochron and depleted mantle Nd model ages or single-grain zircon evaporation Pb–Pb results (Guan, 1996; Ni et al., 2003; Zhang and Li, 1998). However, zircon U–Pb dating by LA-ICPMS reveals that the Muce TTG gneiss (Yiyang area) in the eastern part of the Taihua Complex in the Xiong'er area has crystallization ages of 2.32–2.34 Ga (Diwu et al., 2007). Thus it may be different from the Taihua Complex in the Lushan area, since the latter mostly formed during the Late Mesoarchean to Early Neoarchean (Huang et al., 2010; Liu et al., 2009), indicating the geotectonic setting in southern TNCO might have changed in the Early Paleoproterozoic. In this study, we present

whole rock geochemical and Nd isotopes, and in-situ zircon U–Pb age and Hf isotope data for the gray gneisses from the Taihua Complex in the Xiong'er area in order to: (1) document the emplacement ages of these rocks, (2) investigate their magma sources and petrogenetic processes, and (3) evaluate the Early Paleoproterozoic tectonic evolution of the southern TNCO.

2. Geological background and samples

The North China Craton (NCC; Fig. 1a) is the oldest known cratonic block in China (~3.8 Ga; Liu et al., 1992), with widespread Archean to Paleoproterozoic rocks (Fig. 1a; Zhao et al., 2003). It can be divided into the Eastern and Western Blocks separated by the TNCO (Fig. 1a) on the basis of lithological, structural, metamorphic and geochronological differences (Zhao et al., 2000, 2001). The Western Block can be subdivided into the Ordos Block in the south and the Yinshan Block in the north, which are considered to have amalgamated along the east–west-trending Khondalite Belt at ~1.95 Ga (e.g., Xia et al., 2006; Yin et al., 2009, 2011; Zhao et al., 2005). The late Archean basement of the Eastern and Western blocks is dominated by Neoarchean TTG gneiss domes surrounded by minor supracrustal rocks that underwent greenschist to granulite facies metamorphism at ~2.5 Ga (Zhao et al., 2005). The TNCO represents the collision zone between the two blocks, formed at ~1.85 Ga (e.g., Guo et al., 2005; Liu et al., 2006; Xiao et al., 2011; Zhao et al., 2002). The Archean rocks exposed in the southern segment of TNCO are represented by the Dengfeng and Taihua "groups" (also referred as the Dengfeng Complex and the Taihua Complex, respectively; Zhang et al., 1985).

The Taihua "group" in the Xiong'er area was traditionally considered a meta-volcano-sedimentary sequence (Zhang and Li, 1998; Guan, 1996; Ni et al., 2003), divided into the Caogou, Shiban'gou and Duan'gou "Formations" from the bottom upwards (Zhang and Li, 1998). The Caogou "Formation" consists of dominant meta-felsic magmatic rocks (biotite-plagioclase gneiss) and subordinate meta-mafic magmatic rocks (amphibolite). The Shiban'gou "Formation", the most widespread sequence of the Taihua "group" in the Xiong'er area, consists dominantly of meta-mafic to intermediate magmatic rocks (amphibole-bearing gneiss and amphibolite) and subordinate meta-felsic magmatic rocks (biotite-plagioclase gneiss or granulite). The Duan'gou "Formation" consists dominantly of biotite ± garnet gneiss or granulite, and is a suite of meta-felsic volcanic and sedimentary rocks. The Cao'gou "Formation" is covered by the Shiban'gou

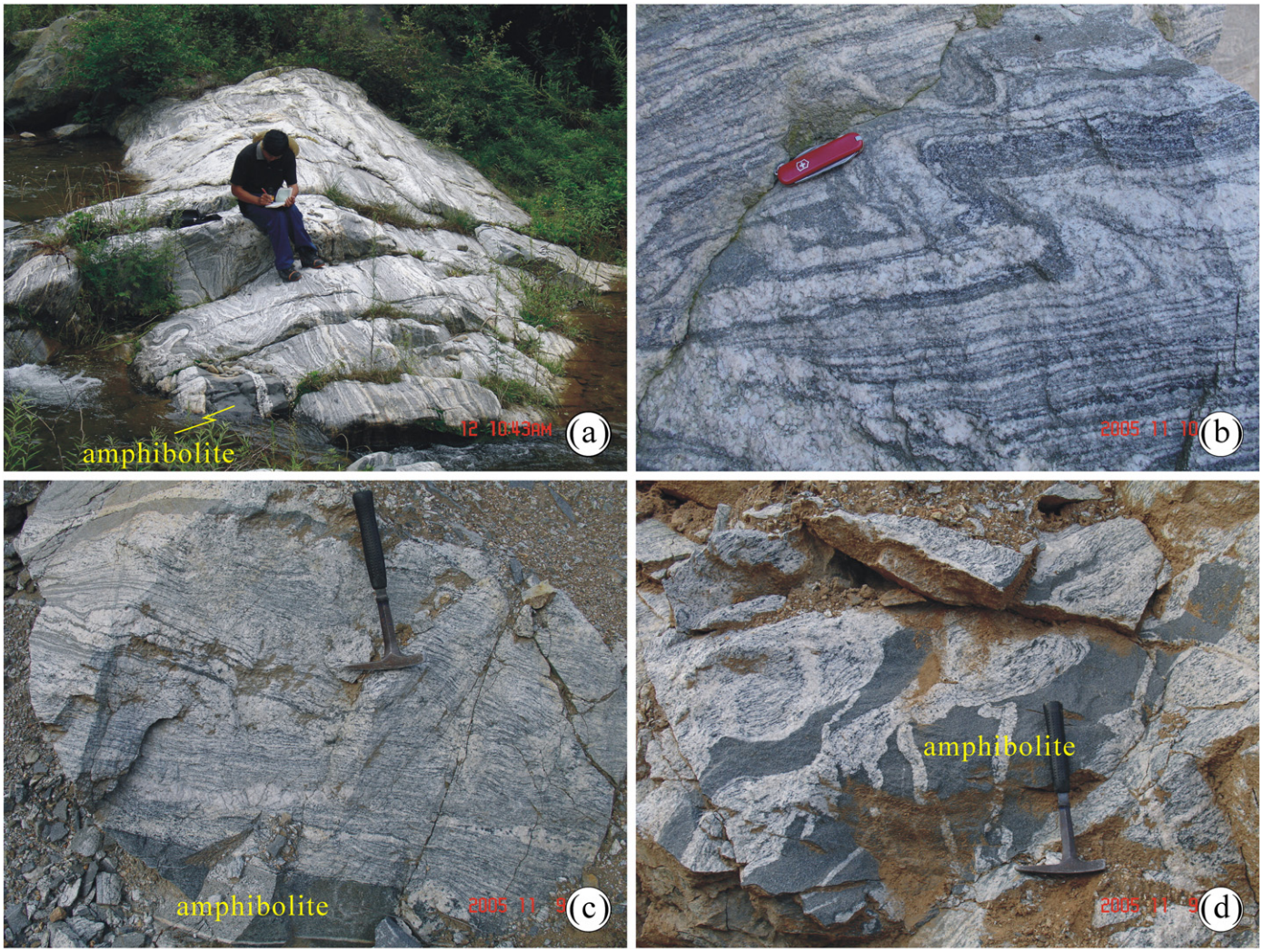

Fig. 2. Field photographs: (a) outcrop of elongated amphibolite enclaves parallel to the banded gray gneiss fabric (Tieluping); (b) banded gray gneiss consisting of parallel light and dark colored gneissose layers (Ganshugou), "cut through" by a light-colored vein at left bottom; (c) the light-colored veins (granite containing predominantly quartz and alkali feldspar, with some biotite) are parallel to the gneissose banding; the lowest part is an elongated amphibolite enclave (Ganshugou); (d) light-colored veins "cut through" the gneissose banding and amphibolite enclaves (Ganshugou). The width of (a) is about 4 m; the length of knife in (b) is 5.8 cm and that of the hammer in (c) and (d) is 30 cm.

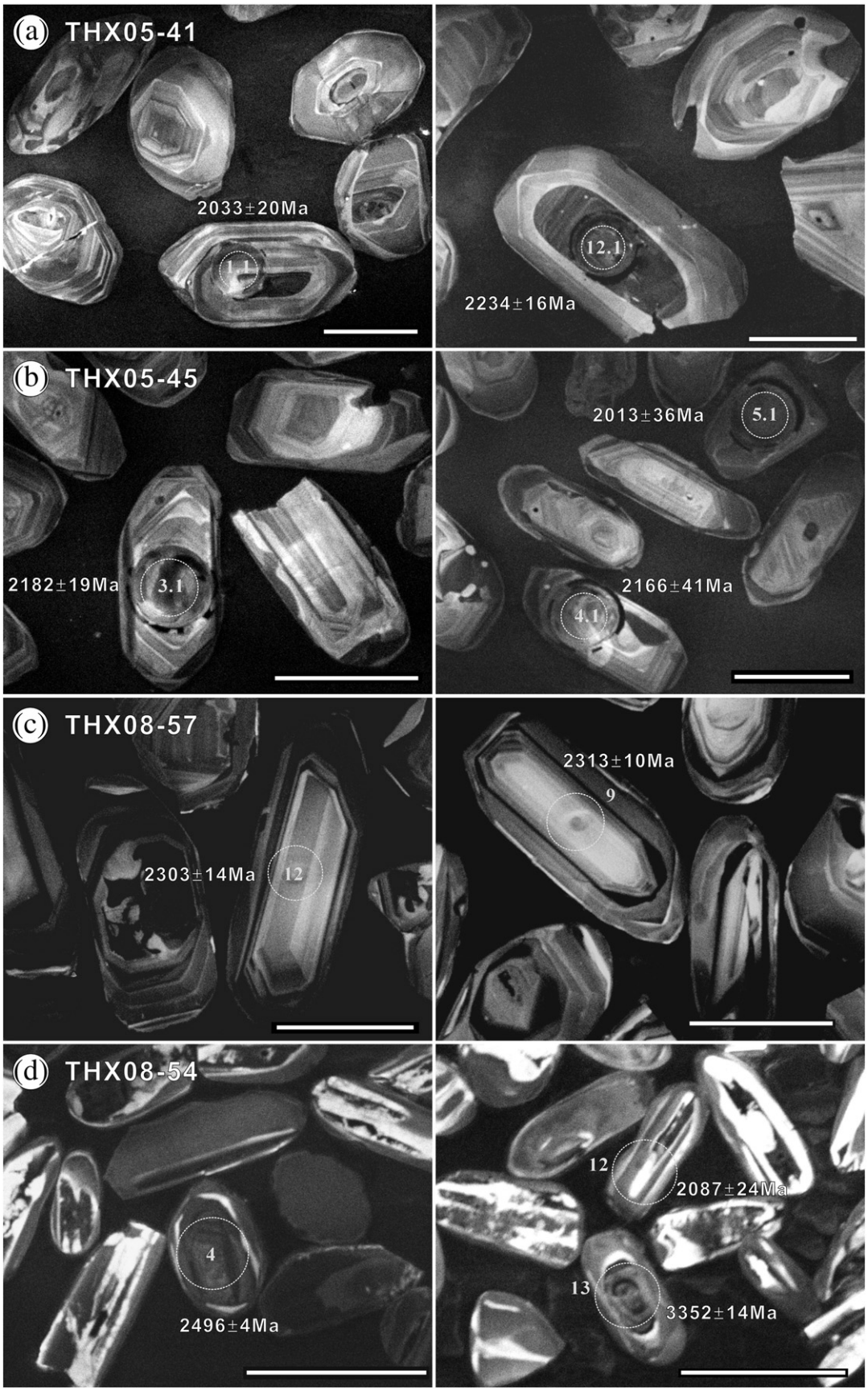

Fig. 3. Cathodoluminescence (CL) images of zircons from (a) tonalite gneiss sample THX05-41 and (b) granite gneiss sample THX05-45 from Ganshugou; (c) granodiorite gneiss sample THX08-57 and (d) diorite gneiss sample THX08-54 from Tieluping. The circles indicate SHRIMP or CAMECA dating sites (30 μm diameter) and laser ablation in-situ zircon Hf isotopic analytical sites (40–50 μm diameter); the scale bar is 100 μm.

"Formation", and the Duan'gou "Formation" unconformably covers the latter (Zhang and Li, 1998). The gneisses of the Taihua Complex in the Xiong'er area are banded (Fig. 2a), consisting of parallel light and dark colored gneissose layers (Fig. 2b). There is widespread "migmatization" and the light-colored veins (granite containing predominant quartz and alkali feldspar with a little mica) are either parallel to the gneissose banding (Fig. 2c) or "cut through" it (Fig. 2b, d). The amphibolites always occur as enclaves in the gneisses (Fig. 2a, c). The Taihua "group" in the Xiong'er area is unconformably or tectonically overlain by the widespread Xiong'er "group" (Fig. 1b) that consists of Late Paleoproterozoic to Early Mesoproterozoic volcanic rocks erupted between 1.78 and 1.45 Ga (He et al., 2009; Wang et al., 2010; Zhao et al., 2009). Cretaceous granite intrudes the Taihua Complex in the Xiong'er area and separates it in eastern and western parts (Fig. 1b).

The studied samples were collected from the so-called Shiban'gou "Formation" in the Tieluping and Ganshugou areas of the western part of the complex (Fig. 1b), which is composed dominantly of gneisses with minor amphibolites. Amphibolites consist of amphibole (70–90%), with subordinate plagioclase (5–30%) and biotite (<10%), and show granoblastic textures. The gneisses are also characterized by granoblastic textures, and have typical gneissic layering (Fig. 2) defined by variations in mineral proportions. According to the mineral assemblages, the gneisses can be classified as diorite gneiss (5–20% biotite, 10–30% amphibole, ~55% plagioclase, <5% K-feldspar and quartz), tonalite/trondhjemite gneiss (5–20% biotite, 3–20% amphibole, 60–70% plagioclase, 10–30% quartz), granodiorite gneiss (<5% biotite, <5% amphibole, 40–70% plagioclase, 10–30% K-feldspar and 10–25% quartz), monzonite gneiss (~10% biotite, ~10% amphibole, ~35% plagioclase, ~45% K-feldspar and <5% quartz) and K-feldspar granite gneiss (<5% biotite, <5% amphibole, ~10% plagioclase, 40–50% K-feldspar and 30–50% quartz). The gneisses in the Ganshugou area include tonalite gneiss, monzonite gneiss and K-feldspar granite gneiss, with minor diorite gneiss. In contrast, the gneisses in the Tieluping area are mainly tonalite and granodiorite gneisses, with minor diorite gneiss. Titanite, magnetite and apatite are common accessory minerals (<1%) in both the amphibolites and gneisses. The gneisses at Muce in the east (Fig. 1b), studied by Diwu et al. (2007), are mostly trondhjemite gneiss consisting of 10–15% biotite, 1–5% amphibole, 50–55% plagioclase and 25–30% quartz.

3. Analytical methods

Geochemical and Nd isotopic analyses were carried out at the Guangzhou Institute of Geochemistry, Chinese Academy of Sciences (GIG-CAS). Major element oxides were analyzed using a Rigaku RIX 2000 X-ray fluorescence spectrometer (XRF), and analytical uncertainties are mostly between 1% and 5% (Li et al., 2006). Trace elements were obtained by inductively coupled plasma-mass spectrometry (ICP-MS), and detailed procedures are described by Li et al. (2006). Precision of REE and other incompatible element analyses is estimated to be better than 5% from the international USGS reference sample BIR-1 and the laboratory standard (ROA-1). In-run analytical precision for Nd is better than 2.5% RSD (relative standard deviation). The Sm/Nd ratios measured by ICP-MS are within 2% uncertainty, and calculation of $\varepsilon_{Nd}(t)$ values for the samples in the present study results in uncertainties of less than 0.25 epsilon units. Nd isotopic analyses were performed on a Micromass Isoprobe multi-collector ICP-MS, using analytical procedures described by Li et al. (2006). REE were separated using cation exchange columns, and Nd

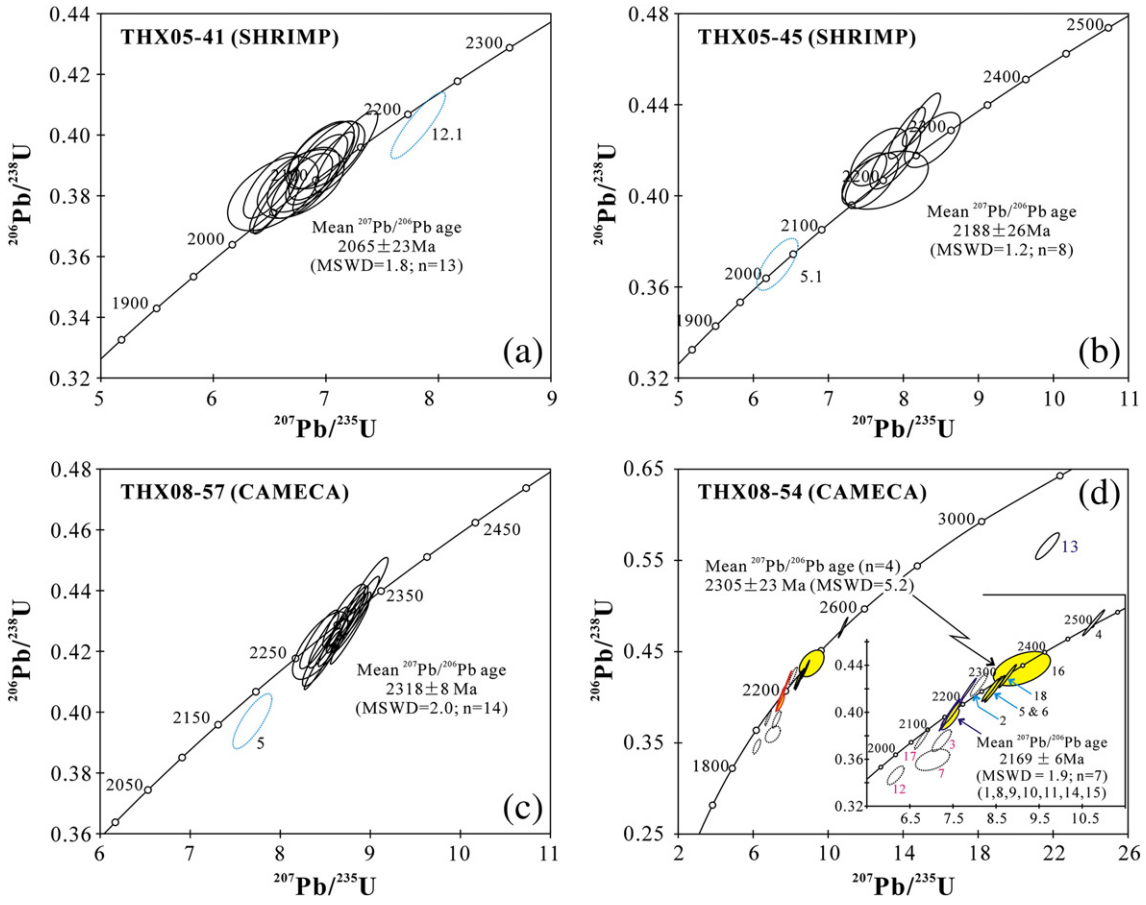

Fig. 4. Concordia diagrams for zircon SHRIMP/CAMECA 1280 U–Pb geochronology of the gray gneisses from the Xiong'er–Taihua Complex. (a) Tonalite gneiss sample THX05-41 and (b) granite gneiss sample THX05-45 from Ganshugou; (c) granodiorite gneiss sample THX08-57 and (d) diorite gneiss sample THX08-54 from Tieluping.

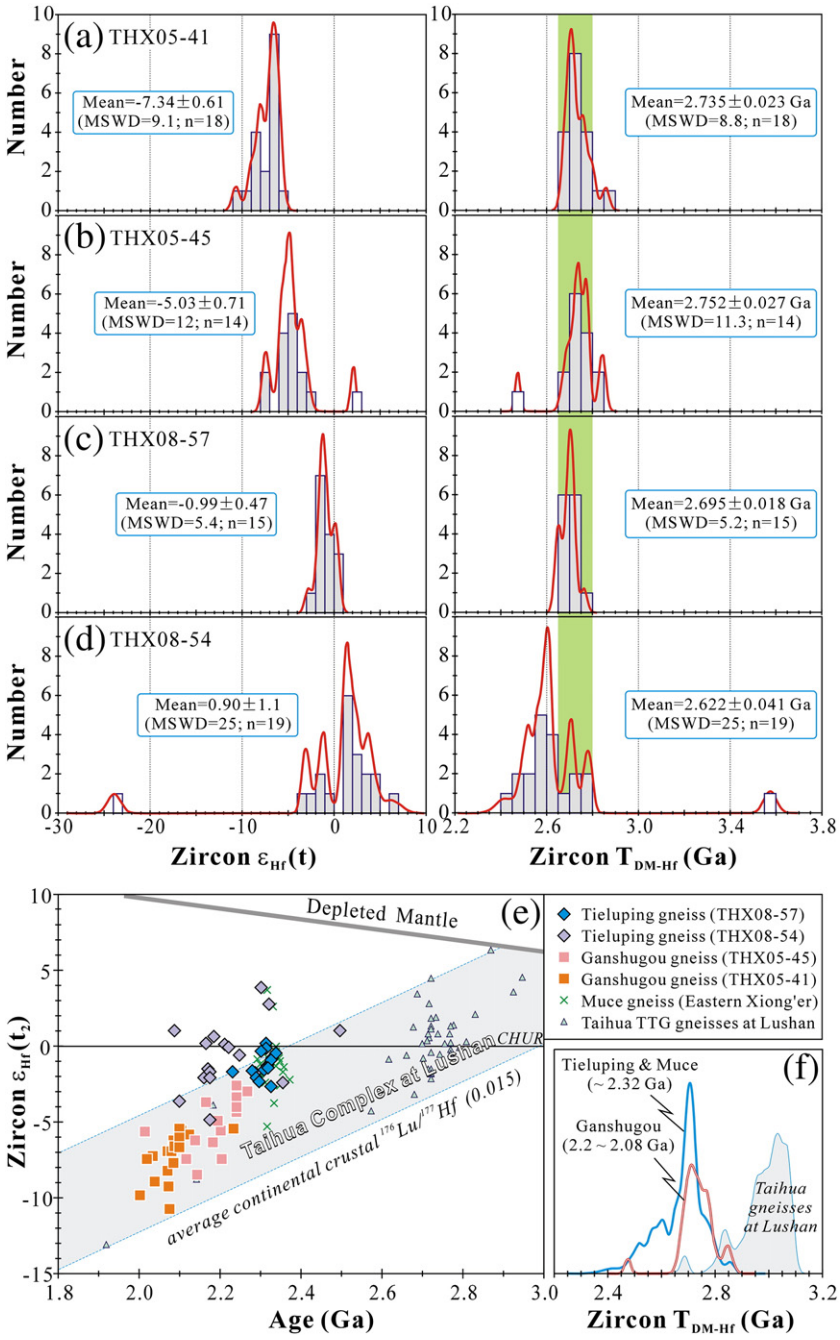

Fig. 5. $\varepsilon_{Hf}(t)$ values and Hf model ages for zircons from gray gneisses of the Taihua Complex at Xiong'er. (a, b, c, d) histograms of $\varepsilon_{Hf}(t)$ and single-stage depleted mantle zircon Hf model ages; t = 2.07 Ga (THX05-41), 2.19 Ga (THX05-45) and 2.32 Ga (THX08-54 and THX08-57); (e) diagram of Hf isotope evolution; t_2 are apparent $^{207}Pb/^{206}Pb$ ages by U–Pb dating (Supplemental Tables 1, 2); the evolution of depleted mantle (DM) is drawn by using present-day $^{176}Hf/^{177}Hf = 0.28325$ and $^{176}Lu/^{177}Hf = 0.0384$ (Griffin et al., 2000). Data sources: the Muce gneiss at the eastern Xiong'er (Diwu et al., 2007), the Taihua Complex at Lushan (Huang et al., 2010).

fractions were further separated by HDEHP-coated Kef columns. Measured $^{143}Nd/^{144}Nd$ ratios were normalized to $^{146}Nd/^{144}Nd = 0.7219$. The reported $^{143}Nd/^{144}Nd$ ratios were adjusted to the Shin Etsu JNdi-1 standard $^{143}Nd/^{144}Nd = 0.512115$.

Zircons were separated using conventional heavy liquid and magnetic techniques and purified by hand-picking under a binocular microscope. They were mounted together with the standard zircon (TEMORA) in epoxy resin. The mount was polished to exposure the grain centers and then gold-coated. The internal structure of the zircons was examined using cathodoluminescence (CL) images prior to U–Pb isotopic analyses. Zircon U–Pb analyses of two samples from Ganshugou (THX05-41 and THX05-45) were performed using a Sensitive High-Resolution Ion Microprobe (SHRIMP II) at the Beijing SHRIMP Center (the Institute of Geology, Chinese Academy of Geological Sciences, Beijing); analytical procedures are similar to those described by Williams (1998). The TEMORA zircon (age 417 Ma) was used for correction of inter-element fractionation and U, Th and Pb concentrations were determined based on the standard Sri Lankan gem zircon SL13, which has a U concentration of 238 ppm and an age of 572 Ma. The Squid (ver. 1.04) and Isoplot (ver. 3.23) programs (Ludwig, 2003) were used for raw data reduction and age calculation, and common lead was corrected using the measured ^{204}Pb. Uncertainties reported in Supplemental Table 1 are all $\pm 1\sigma$. The weighted mean ages quoted in the text ($^{207}Pb/^{206}Pb$ ages) are at the 95% confidence level. Zircon U–Pb analyses of two samples from Tieluping (THX08-54 and THX08-57) were performed on the CAMECA IMS

Table 1
Major (wt.%) and trace element (ppm) data of the Taihua Complex in the Xiong'er area.

Sample	THX05-40	THX05-41	THX05-43	THX05-44	THX05-45	THX05-46	THX08-28	THX08-29	THX08-35	THX05-42
Rocks	Tonalite gneiss	Tonalite gneiss	Diorite gneiss	Kfs. granite gneiss	Kfs. granite gneiss	Monzonite gneiss	Diorite gneiss	Tonalite gneiss	Monzonite gneiss	Amp.
Location	Ganshugou	Ganshugou	Ganshugou	Ganshugou	Ganshugou	Ganshugou	Ganshugou	Ganshugou	Ganshugou	Ganshugou
SiO_2	62.97	55.51	61.56	69.64	74.68	64.69	54.07	57.35	65.58	50.21
TiO_2	0.48	1.06	1.00	0.38	0.22	0.68	1.50	1.38	0.49	4.40
Al_2O_3	16.98	16.56	15.69	14.41	12.38	15.14	16.15	15.49	15.61	13.22
Fe_2O_3	5.65	8.46	7.61	4.41	2.87	6.50	8.66	7.72	3.76	13.78
MnO	0.11	0.13	0.10	0.04	0.03	0.07	0.15	0.11	0.05	0.19
MgO	1.83	3.89	1.53	0.28	0.10	1.25	3.44	3.29	1.37	5.55
CaO	4.37	4.46	3.71	1.65	1.13	3.32	5.50	5.43	2.42	8.06
Na_2O	3.29	3.66	3.56	2.60	2.59	2.50	4.09	3.63	3.61	2.40
K_2O	2.64	3.80	4.06	5.76	5.05	4.21	3.80	3.36	5.54	1.46
P_2O_5	0.15	0.46	0.48	0.07	0.03	0.21	0.60	0.79	0.14	0.17
LOI	1.20	1.58	0.33	0.49	0.21	0.83	1.84	1.34	1.24	0.52
Total	99.69	99.57	99.65	99.73	99.30	99.40	99.79	99.88	99.81	99.96
$Mg^{\#}$	0.43	0.52	0.32	0.13	0.08	0.31	0.48	0.50	0.46	0.48
Sc	9.27	14.6	10.0	6.37	2.45	12.2	13.4	12.7	6.17	23.0
Ti	3150	6323	6150	2342	1303	4200	8947	8113	2680	26245
V	73.5	113	44.0	10.2	6.81	35.2	120	109	43.8	227
Cr	5	104	3	1	5	6	40	44	28	272
Co	13.1	20.7	11.1	3.37	2.25	9.13	31.5	38.7	28.2	42.8
Ni	5	43	4	1	1	4	27	30	14	66
Cu	22.3	28.9	20.1	12.6	11.0	17.5	83.9	57.4	4.34	67.3
Zn	80	107	116	42	35	82	106	99	56	145
Ga	19.6	23.8	22.6	22.3	16.5	18.8	22.3	22.8	20.0	19.1
Ge	1.33	1.47	1.69	1.65	1.28	1.35	1.34	1.25	1.24	1.72
Rb	67	114	161	122	149	108	106	91	161	36
Sr	551	508	547	199	121	366	726	986	561	364
Y	19.8	25.4	30.1	51.3	19.0	18.2	19.0	22.1	15.0	20.2
Zr	185	442	524	442	248	235	190	191	307	135
Nb	9.19	23.2	26.7	17.4	9.59	9.14	17.2	18.8	13.1	23.8
Ba	1373	1195	1592	1528	1064	1518	1677	1944	1433	283
Hf	4.25	10.3	11.84	11.6	6.98	5.82	4.32	4.77	8.13	3.35
Ta	0.45	1.46	1.34	0.52	0.29	0.28	1.18	1.24	0.88	1.84
Pb	15.5	20.3	27.5	28.2	23.4	20.5	17.8	19.4	34.0	6.83
Th	3.02	20.9	14.7	38.8	9.70	5.25	8.75	15.3	56.9	0.84
U	0.20	3.43	3.79	2.28	1.03	0.58	2.24	2.61	6.52	0.48
La	24.8	64.4	104	136	32.8	46.9	64.7	88.6	60.9	14.9
Ce	51.6	128	205	285	65.1	94.7	131	173	113	37.1
Pr	6.61	15.6	26.1	31.8	7.88	11.4	15.1	19.0	11.8	5.64
Nd	25.7	54.5	90.4	106	28.4	40.5	57.1	68.5	39.0	23.6
Sm	4.95	8.98	13.8	17.3	5.30	7.15	8.39	9.77	5.43	5.82
Eu	1.48	1.68	2.79	2.34	1.34	1.63	2.09	2.08	1.31	1.73
Gd	4.54	6.54	10.1	12.8	4.57	5.91	6.60	7.91	4.26	5.09
Tb	0.66	0.88	1.14	1.88	0.71	0.75	0.80	0.92	0.50	0.78
Dy	3.69	4.64	5.93	9.90	3.72	3.79	3.92	4.38	2.65	3.99
Ho	0.75	0.91	1.09	2.03	0.76	0.68	0.73	0.81	0.53	0.76
Er	2.05	2.51	2.85	5.70	1.98	1.80	1.87	2.15	1.49	1.97
Tm	0.30	0.39	0.42	0.83	0.27	0.24	0.26	0.31	0.23	0.29
Yb	1.83	2.44	2.72	5.59	1.86	1.38	1.69	2.00	1.57	2.03
Lu	0.28	0.38	0.40	0.84	0.25	0.18	0.26	0.31	0.25	0.30
Eu/Eu^*	0.97	0.80	0.83	0.68	0.90	0.86	0.91	0.84	0.90	0.98
$(La/Yb)_N$	9.2	17.8	25.7	16.4	11.9	23.1	25.9	30.0	26.3	5.0
Sr/Y	27.9	20.0	18.2	3.9	6.4	20.1	38.3	44.6	37.5	18.1
Dy/Yb	2.01	1.90	2.18	1.77	2.00	2.75	2.32	2.19	1.69	1.97
Rb/Sr	0.12	0.22	0.29	0.61	1.23	0.30	0.15	0.09	0.29	0.10

Abbreviations: K-feldspar (Kfs.); amphibolite (Amp.).

1280 ion microprobe at the Institute of Geology and Geophysics, Chinese Academy of Sciences (IGG-CAS) in Beijing, China. Analytical procedures are similar to those described by Li et al. (2009). U–Th–Pb isotopic ratios and absolute abundances were determined relative to the standard zircon 91500 (Wiedenbeck et al., 1995). Measured Pb isotopic compositions were corrected for common Pb using the measured ^{204}Pb. Uncertainties on individual analyses in Supplemental Table 2 are reported at the 1σ level; data reduction was carried out using Isoplot (ver. 3.23) (Ludwig, 2003).

In-situ zircon Hf isotopic analyses were carried out on the dated sites using a Neptune MC-ICPMS, equipped with a 193 nm laser, at IGG-CAS. Spot sizes of 40 μm with a laser repetition rate of 8 Hz at 100 mJ were used. The detailed analytical technique and data correction procedures are described in Wu et al. (2006). During analysis of the unknown samples, the zircon standard (91500) gave $^{176}Hf/^{177}Hf = 0.282292 \pm 14$ (2σ) and $^{176}Lu/^{177}Hf = 0.00029$, similar to the $^{176}Hf/^{177}Hf$ ratios of 0.282284 ± 22 reported by Griffin et al. (2006).

STHX08-39	THX05-49	THX05-53	THX05-55	THX08-51	THX08-54	THX08-55	THX08-57	THX08-59	THX08-60
Amp.	Toanlite gneiss	Tonalite gneiss	Tonalite gneiss	Grano-diorite gneiss	Diorite gneiss	Tonalite gneiss	Grano-diorite gneiss	Grano-diorite gneiss	Grano-diorite gneiss
Ganshugou	Tieluping	Tieluping	Tieluping	Tieluping	Tieluping	Tieluping	Tieluping	Tieluping	Tieluping
50.11	67.63	68.28	67.74	71.67	54.61	62.20	69.65	72.32	69.12
3.73	0.39	0.40	0.30	0.36	0.79	0.59	0.31	0.35	0.32
14.45	16.10	15.40	16.99	15.16	16.95	16.56	15.58	13.76	15.43
12.91	4.08	3.78	2.98	1.67	8.80	5.77	2.68	1.97	3.14
0.16	0.04	0.04	0.03	0.01	0.13	0.07	0.04	0.02	0.04
4.48	1.44	1.70	0.93	0.66	4.32	1.88	1.11	0.60	1.38
7.97	3.53	2.78	3.26	2.58	6.76	4.86	3.08	1.30	3.31
3.18	3.48	3.26	4.45	4.42	4.06	4.13	3.93	2.63	3.90
1.29	2.35	3.71	2.24	2.21	1.98	2.11	3.12	5.93	2.66
0.38	0.11	0.09	0.10	0.06	0.38	0.14	0.09	0.08	0.12
0.93	0.82	0.32	0.77	0.78	1.30	2.03	0.78	0.82	0.94
99.58	99.97	99.77	99.79	99.58	100.08	100.35	100.36	99.78	100.34
0.45	0.45	0.51	0.42	0.48	0.53	0.43	0.49	0.42	0.51
24.3	5.38	4.50	3.64	2.05	14.4	4.73	5.13	3.82	6.56
22149	2437	2343	1733	1934	4140	2454	1631	1889	1711
192	54.7	46.4	34.1	25.9	82.9	44.5	30.4	15.5	44.2
123	26	21	6	4	38	10	13	4	19
47.8	10.2	8.41	5.98	20.6	32.0	20.1	24.0	24.4	30.8
37	17	17	8	3	12	10	10	3	11
41.7	20.0	20.8	21.2	2.46	18.7	19.0	3.55	1.39	18.5
151	51	48	48	39	92	46	35	27	40
22.8	19.2	17.5	20.1	21.6	20.7	21.5	17.6	16.4	18.6
1.67	1.02	0.95	0.83	0.62	1.26	0.88	0.96	0.86	0.91
25	86	102	63	34	53	59	67	112	70
471	398	469	512	451	777	446	494	339	416
26.4	5.40	7.55	10.2	2.05	13.2	6.20	9.96	8.82	10.7
202	131	135	141	142	112	105	135	287	97.3
27.9	9.04	4.96	7.81	2.09	5.48	4.50	5.74	5.73	7.30
262	868	1716	1076	777	967	447	1128	2547	927
5.07	3.59	3.62	3.45	3.72	2.70	2.49	3.48	7.31	2.71
2.25	0.21	0.44	0.38	0.14	0.37	0.19	0.31	0.14	0.37
10.5	21.9	28.4	32.0	19.8	10.5	11.5	14.3	25.4	20.1
1.43	10.5	11.4	4.36	6.36	3.07	4.95	7.32	28.2	8.85
0.75	1.13	0.59	0.53	0.23	0.81	0.38	0.41	1.53	0.66
26.2	31.7	40.4	23.9	34.7	25.0	23.5	24.9	163	20.9
65.8	59.0	72.5	40.6	62.9	53.5	48.8	47.9	328	41.9
8.84	6.56	8.46	4.70	6.58	6.56	5.39	5.19	29.5	4.61
37.4	21.6	27.9	16.0	23.4	26.6	19.4	18.7	92.9	16.8
8.28	3.38	4.29	2.70	3.20	4.80	3.19	3.12	10.9	2.95
2.21	0.80	1.07	1.11	0.93	1.42	0.65	0.81	1.21	0.69
7.30	2.57	3.04	2.37	1.97	3.87	2.56	2.57	7.37	2.77
1.06	0.29	0.35	0.31	0.15	0.51	0.29	0.34	0.59	0.38
5.47	1.27	1.58	1.75	0.51	2.60	1.32	1.84	2.20	2.00
1.02	0.22	0.29	0.38	0.067	0.49	0.23	0.35	0.32	0.39
2.56	0.48	0.75	1.09	0.17	1.30	0.56	0.95	0.77	1.03
0.36	0.063	0.097	0.16	0.021	0.18	0.071	0.14	0.086	0.13
2.39	0.37	0.64	0.98	0.14	1.18	0.43	0.88	0.57	0.86
0.37	0.052	0.092	0.14	0.021	0.17	0.064	0.14	0.095	0.12
0.92	0.89	0.93	1.14	1.03	0.99	0.82	0.92	0.62	0.85
7.4	58.7	42.9	16.5	164.1	14.3	36.8	19.1	192.6	16.5
17.9	73.7	62.0	50.0	220.1	58.7	71.9	49.6	38.5	38.8
2.29	3.48	2.47	1.79	3.54	2.21	3.05	2.08	3.83	2.33
0.05	0.22	0.22	0.12	0.07	0.07	0.13	0.14	0.33	0.17

4. Results

4.1. Zircon U–Pb geochronology and Hf isotopes

4.1.1. In-situ zircon U–Pb dating

Two samples from Ganshugou (tonalite gneiss THX05-41 and granite gneiss THX05-45) and two samples from Tieluping (granodiorite gneiss THX08-57 and diorite gneiss THX08-54) were selected for zircon U–Pb dating by SHRIMP and CAMECA 1280, respectively. The zircons from samples THX05-41, THX05-45 and THX08-57 are mostly euhedral prismatic or long-prismatic grains with sharp terminations (Fig. 3a, b, c). As shown by CL images, these zircons have well developed oscillatory zoning, but some also have structureless rims (Fig. 3a, b, c). The zircons of diorite sample THX08-54 from Tieluping are all subhedral and slightly rounded; CL images show that some zircons retain oscillatory zoning in the centers, whereas other zircons have no obvious oscillatory zoning or are structureless (Fig. 3d).

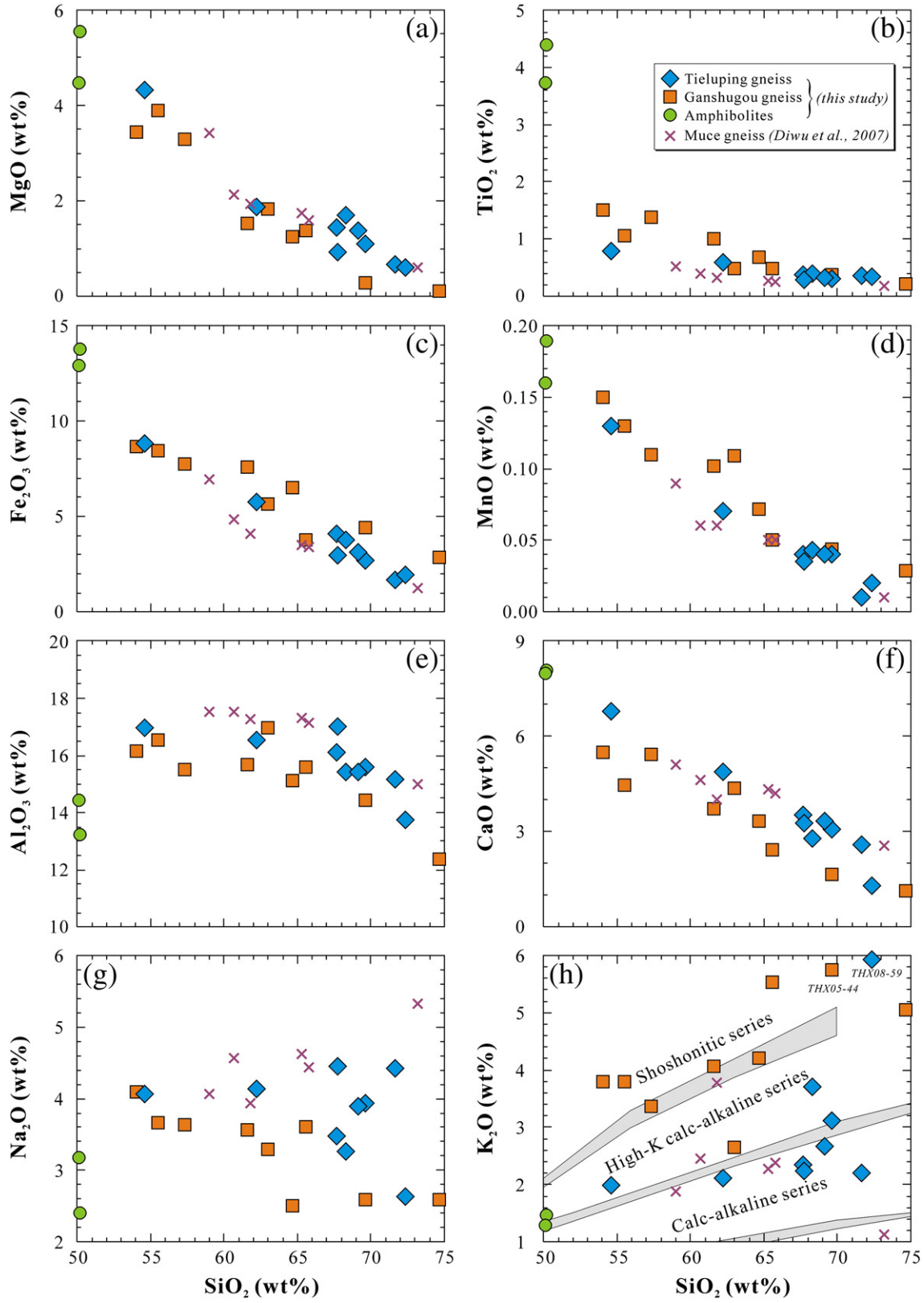

Fig. 6. SiO_2 variation diagrams of representative major element oxides for the Taihua gneisses and amphibolites at the western Xiong'er compared with the Muce gneisses at the eastern Xiong'er from Diwu et al. (2007).

4.1.1.1. Sample THX05-41 (tonalite gneiss). Fourteen zircons from sample THX05-41 were analyzed in cores with distinct oscillatory zoning. The zircons contain moderate Th and U contents (104–337 ppm and 62–300 ppm, respectively) with high Th/U ratios of 0.62–1.05 (Supplemental Table 1). Most analyses have low common lead with $f_{206}<0.41\%$ except for one giving f_{206} of 0.75% (Supplemental Table 1). Thirteen U–Pb results are concentrated on concordia and yield a weighted mean $^{207}Pb/^{206}Pb$ age of 2065 ± 23 Ma (MSWD = 1.8)

(Fig. 4a), which is interpreted as the best estimate of the magmatic age of the tonalite gneiss protolith. One analysis (Spot 12.1) on a core (Fig. 3a) gives an older apparent $^{207}Pb/^{206}Pb$ age of 2234 ± 16 Ma (Supplemental Table 1; Fig. 4a).

4.1.1.2. Sample THX05-45 (K-feldspar granite gneiss). The analyzed spots on oscillatory zoned cores all have high Th/U ratios of 0.42–0.76 with moderate Th and U contents (136–619 ppm and 72–292 ppm, respectively; Supplemental Table 1). These data-points yield a weighted mean $^{207}Pb/^{206}Pb$ age of 2188 ± 26 Ma (MSWD = 1.2) (Fig. 4b), which is interpreted as the magmatic crystallization age of the K-feldspar granite gneiss protolith. Spot 5.1 on a structureless zircon core (Fig. 3b) gives a younger apparent $^{207}Pb/^{206}Pb$ age of 2013 ± 36 Ma (Supplemental Table 1; Fig. 4b), which may record metamorphic recrystallization, since it has a low Th/U ratio of 0.05 (Supplemental Table 1).

4.1.1.3. Sample THX08-57 (granodiorite gneiss). Fifteen analyses were made on oscillatory zoned cores of 15 zircon grains. They contain low to moderate U and Th contents (54–284 ppm and 33–222 ppm, respectively) with high Th/U ratios of 0.53–1.00 (Supplemental Table 2). Except for Spot 5 with the lowest Th/U ratio of 0.53, the others define a single population that gives a weighted mean $^{207}Pb/^{206}Pb$ age of 2318 ± 8 Ma (MSWD = 2.0) (Fig. 4c), interpreted to be the crystallization age of the gneissic protolith.

4.1.1.4. Sample THX08-54 (diorite gneiss). Most zircons in this sample lack oscillatory zoning, are structureless or have banded zones. Eleven analyses (Spots 1, 2, 3, 7, 8, 9, 10, 11, 12, 14, 15 and 17) show relatively low Th/U ratios (lower than 0.10 except for spots 1 and 12). Seven of them define a population that gives a weighted mean $^{207}Pb/^{206}Pb$ age of 2169 ± 6 Ma (MSWD = 1.9) (Fig. 4d), which can be interpreted to reflect the metamorphic age of gneisses in the Tieluping area. The other analyses (Spots 4, 5, 6, 13, 16 and 18) made on cores with banded zones have high Th/U ratios (0.45–0.95) and give variable apparent $^{207}Pb/^{206}Pb$ age from 2286 ± 7 Ma to 3352 ± 14 Ma (Supplemental Table 2; Fig. 4d). Except for spots 4 and 13, the remaining four analyses give a weighted mean $^{207}Pb/^{206}Pb$ age of 2305 ± 23 Ma (MSWD = 5.2) similar to the crystallization age of Sample THX05-57 (2318 ± 8 Ma) within error.

4.1.2. LA-MC-ICPMS Lu–Hf isotopes

Most zircons analyzed for Lu–Hf were previously dated by SHRIMP or CAMECA 1280 on the same sites (Supplemental Table 3). The initial Hf isotope ratios were calculated at the crystallization age (t) and $^{207}Pb/^{206}Pb$ age (t_2) determined for that site, respectively (Supplemental Table 3), and the single-stage Hf model ages ($T_{DM\text{-}Hf}$) are referenced to depleted mantle (Supplemental Table 3; Fig. 5), whereas the "crustal" model ages ($T^{C}_{DM\text{-}Hf}$) were calculated by assuming the parental magma was produced from average continental crust ($^{176}Lu/^{177}Hf = 0.015$) that originally was derived from the depleted mantle (Griffin et al., 2004).

4.1.2.1. Sample THX05-41. The zircons have $^{176}Hf/^{177}Hf$ ratios ranging from 0.281188 to 0.281349, with negative $\varepsilon_{Hf}(t)$ (−10.7 to −5.9) at 2.08 Ga. The single-stage Hf model ages range from 2678 to 2858 Ma and the "crustal" model ages range from 3039 to 3330 Ma.

4.1.2.2. Sample THX05-45. The zircon $^{176}Hf/^{177}Hf$ ratios range from 0.281205 to 0.281473, with variable $\varepsilon_{Hf}(t)$ values (−5.9–2.1) at 2.19 Ga. Except for Spot 05 corresponding to the SHRIMP U–Pb dating Spot 5.1 on a structureless zircon, the single-stage Hf model ages range from 2674 to 2843 Ma and the "crustal" model ages from 2948 to 3231 Ma (Supplemental Table 3). They are overall similar to those of sample THX05-41.

4.1.2.3. Sample THX08-57. The zircons have fairly uniform $^{176}Hf/^{177}Hf$ ratios of 0.281259–0.281355, corresponding to $\varepsilon_{Hf}(t)$ values of −2.8–0.3 (mean value −0.86 ± 0.41) at 2.32 Ga. The single-stage Hf model ages range from 2646 to 2763 Ma (mean value 2695 ± 18 Ma) and the "crustal" model ages from 2843 to 3031 Ma (mean value 2915 ± 25 Ma) (Supplemental Table 3).

4.1.2.4. Sample THX08-54. Except for the oldest inherited zircon, the zircon $^{176}Hf/^{177}Hf$ ratios mostly vary from 0.281257 to 0.281519, corresponding to variable $\varepsilon_{Hf}(t)$ values of −3.21–6.22 at 2.32 Ga. The single-stage Hf model ages range from 2420 to 2790 Ma and the "crustal" model ages from 2480 to 3058 Ma (Supplemental Table 3); the oldest inherited zircon (Spot 13c) has the lowest $^{176}Hf/^{177}Hf$ (0.280684 ± 41) with $\varepsilon_{Hf}(t)$ value of −23.91 at 2.32 Ga, and the oldest single-stage Hf model age (3575 ± 55 Ma) and "crustal" model age (3707 ± 55 Ma) (Supplemental Table 3).

Despite the variable zircon ε_{Hf} (t) values, samples THX05-41, THX05-45 and THX08-57 have very similar zircon single-stage Hf model ages forming peaks between 2.69 Ga and 2.75 Ga (Fig. 5a, b, c). The single-stage Hf model ages of several zircons from sample THX08-54 are in range of 2.69–2.75 Ga, but most zircons define a younger peak at 2.62 Ga (Fig. 5d). Zircon ε_{Hf} (t_2) values of the Taihua gneisses in the Xiong'er area calculated using the $^{207}Pb/^{206}Pb$ ages are all lower than the depleted mantle value (Griffin et al., 2000) (Fig. 5e). The zircons from the samples from Ganshugou (THX05-41 and THX05-45) define a similar Lu–Hf isotope reservoir to those from the Taihua Complex at Lushan (Huang et al., 2010) by using the crustal $^{176}Lu/^{177}Hf$ value of 0.015 (Fig. 5e). However, the zircons from the samples from Tieluping (THX08-57 and THX08-54) show higher ε_{Hf} (t_2) values and younger "crustal" model ages than those from Ganshugou, and would be derived from a younger reservoir than the Taihua Complex at Lushan (Fig. 5e). As a comparison, the zircons from the Muce TTG gneisses of the Taihua Complex at the eastern Xiong'er (Fig. 1b) (~2.3 Ga; Diwu et al., 2007) show variable reservoirs (Fig. 5e).

4.2. Major and trace elements

Two amphibolite samples from Ganshugou (THX05-42 and THX08-39) contain low SiO_2 (50.1–50.2 wt.%), high MgO (4.48–

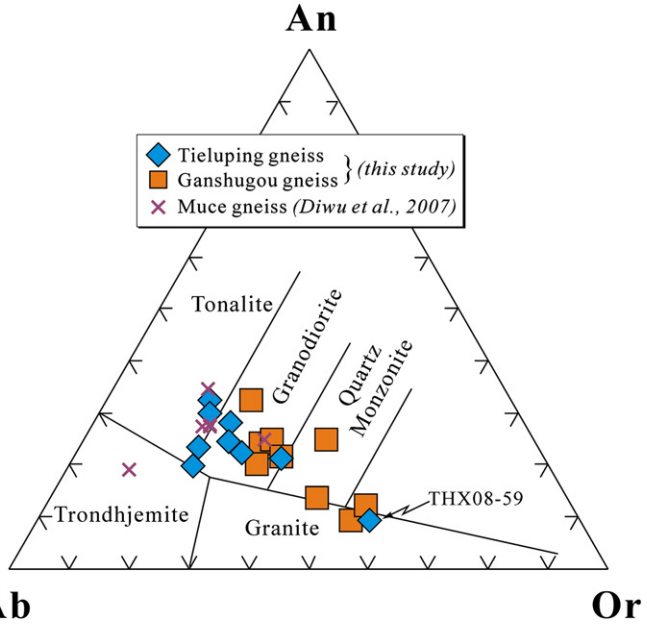

Fig. 7. Normative feldspar composition for the Taihua gneisses at Xiong'er in the An–Ab–Or classification diagram (Barker and Arth, 1976).

5.55 wt.%), Fe_2O_3 (12.9–13.8 wt.%), TiO_2 (3.73–4.40 wt.%) and CaO (7.97–8.06 wt.%) (Table 1). Eighteen gneiss samples (including seven tonalite, three diorite, four granodiorite, two K-feldspar granite and two monzonite gneisses) from Ganshugou and Tieluping contain variable SiO_2 (54.1–74.7 wt.%), MgO (0.10–4.3), Fe_2O_3 (1.67–8.80 wt.%) and CaO (1.13–6.76 wt.%). The Tieluping gneisses have higher Na_2O, Al_2O_3 and CaO but lower K_2O, Fe_2O_3, MnO and TiO_2 than the Ganshugou gneisses for the same amount of SiO_2 (Fig. 6). In the triangular diagram of normative feldspar composition, the Tieluping gneisses, along with the Muce gneisses at the eastern Xiong'er, plot in the fields of trondhjemite, tonalite and granodiorite except for the most felsic sample (THX08-59); the Ganshugou gneisses plot in the fields of granodiorite, quartz monzonite and granite (Fig. 7).

The amphibolites have slightly fractionated REE patterns ($[La/Yb]_N = 4.95 - 7.39$) with weak to negligible negative Eu anomalies (Fig. 8a). On the primitive mantle-normalized multi-element spidergram, the amphibolites show weak positive Ta and Ti anomalies (Fig. 8b). The gneisses from Ganshugou have fractionated LREE and nearly flat HREE patterns ($[La/Yb]_N = 9.15 - 30.0$; $[Dy/Yb]_N = 1.31 - 1.43$) with weak to moderate negative Eu anomalies ($Eu/Eu^* = 0.68 - 0.97$) (Fig. 8a), and show negative Ta–Nb and Ti anomalies (Fig. 8b). Two K-feldspar granitic gneiss samples (THX05-44 and THX05-45) are characterized by very low Sr concentrations and high Nb/Ta ratios (Fig. 8b). Sample THX05-44 has elevated HREE concentrations with negative Eu and Sr anomalies (Fig. 8a, b).

The gneisses from Tieluping show LREE-enriched and HREE-depleted patterns (Fig. 8c). They all have very low HREE ($Yb_N = 0.58 - 4.75$) and Y (2.05–13.2 ppm) with moderate to high $[La/Yb]_N$ (14.3–192.6) and Sr/Y (38.5–220.1). Furthermore, they show variable Eu anomalies ($Eu/Eu^* = 0.62 - 1.14$; Table 1). Sample THX08-59 has very high LREEs with a strong negative Eu anomaly because of the high proportion of K-feldspar (~30%) in the sample. Except for sample THX08-59, the gneisses from Tieluping are characterized by pronounced negative Nb–Ta and Ti anomalies but positive Sr and Pb anomalies (Fig. 8d). In comparison, the gneisses from Muce at the eastern Xiong'er (Diwu et al., 2007) have relatively higher HREE than the Tieluping gneisses, and show typical U-type REE patterns with low MREE (Fig. 8c).

All the gneiss samples from Tieluping plot in the field of adakite and high Al-TTG on the $[La/Yb]_N$ versus Yb_N and Sr/Y versus Y diagrams (Fig. 9). Except for the diorite sample (THX08-54), the gneisses from Tieluping resemble TTGs with high SiO_2, high Na_2O and low ferromagnesian elements (Fig. 6) (Martin et al., 2005). All gneiss samples from Muce (Diwu et al., 2007) and some gneiss samples from Ganshugou also plot in the TTG-adakite field on the $[La/Yb]_N$ versus Yb_N diagram (Fig. 9a). On the Sr/Y versus Y diagram, the gneisses from both the Muce and Ganshugou areas plot away from this field because of higher Y (Fig. 9b). The gneisses from Ganshugou do not belong to TTG because of their low Na_2O and high K_2O (Fig. 6g, h). In contrast, the gneisses from Muce resemble high-Al TTG with features of high Al_2O_3, Na_2O (Fig. 6e, g) and Sr (Fig. 8d) but low K_2O (Fig. 6h).

4.3. Whole rock Nd isotopes

The gneisses from Ganshugou all have negative $\varepsilon_{Nd}(t)$ (-5.01 to -2.33), and single-stage Nd model ages (T_{DM}) vary from 2.55 Ga to 2.81 Ga, which are much older than the crystallization ages of 2.07–2.19 Ga. The amphibolite samples from both the Ganshugou and Tieluping areas have positive $\varepsilon_{Nd}(t)$ values (Table 2) with similar T_{DM} model ages of 2.92–2.94 Ga (Table 2), which are slightly older than

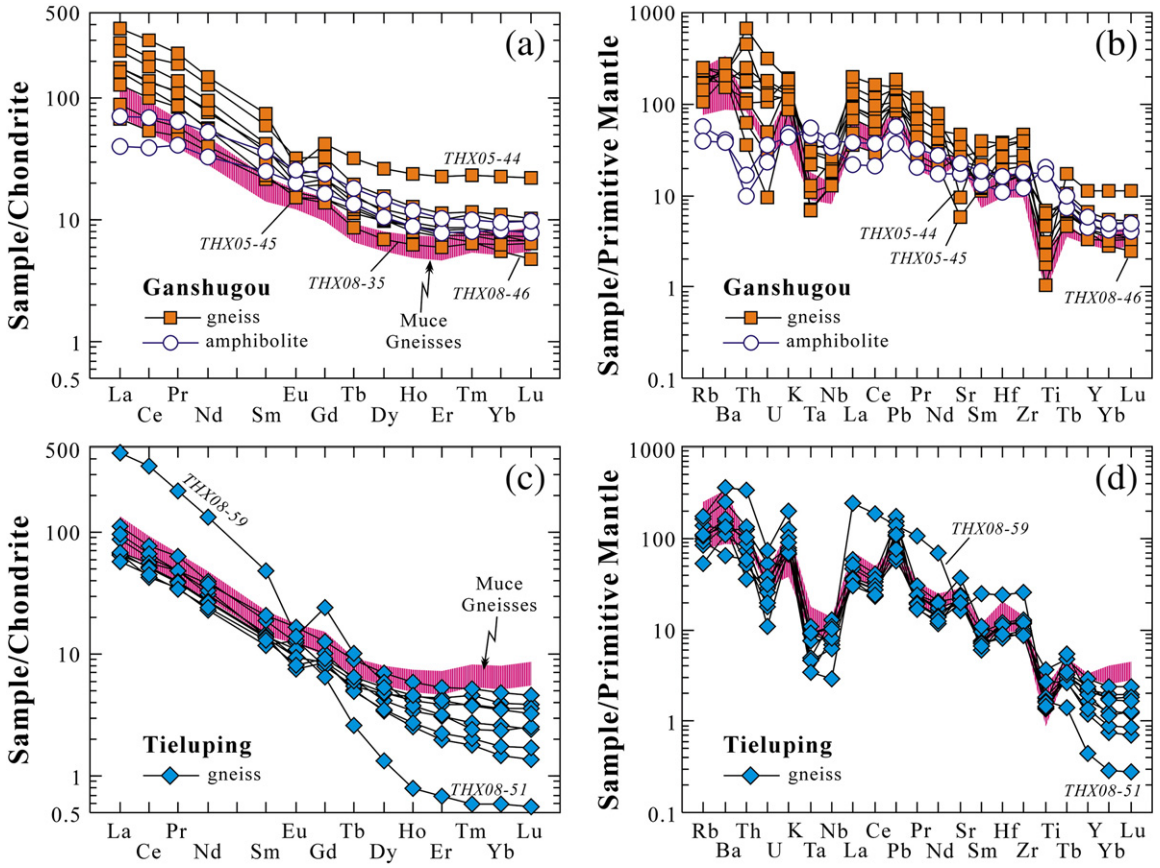

Fig. 8. Chondrite-normalized REE patterns and primitive mantle-normalized trace element spidergrams for amphibolite and gneisses from the Taihua Complex at Xiong'er. (a) REE patterns and (b) spidergrams for amphibolite and gneisses from Ganshugou; (c) REE patterns and (d) spidergrams for gneisses from Tieluping. Chondrite and PM normalization factors are from Taylor and McLennan (1985) and Sun and McDonough (1989). The data for the Muce gneisses are from Diwu et al. (2007).

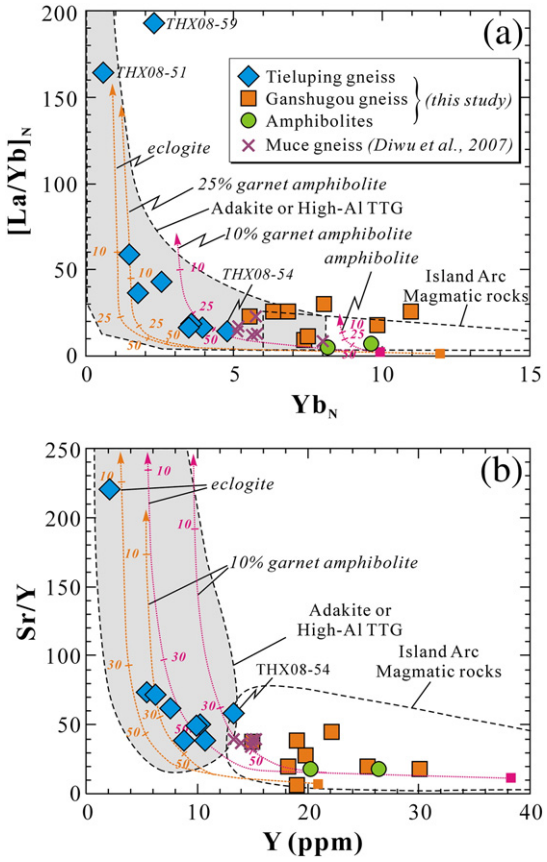

Fig. 9. Plots of (a) $(La/Yb)_N$ vs. Yb_N and (b) Sr/Y vs. Y for the Taihua gneisses and amphibolites in the Xiong'er area. Fields of high-Al TTG, adakite and common island arc magmatic rocks are from Defant and Drummond (1990) and Martin et al. (2005). The partial melting curve is from Drummond and Defant (1990).

the crystallization age (2.68 Ga; Ni et al., 2003) but very close to the T_{DM} model ages of the gneisses in the Taihua Complex at Lushan (2.84–3.11 Ga; Huang et al., 2010). The gneisses from Tieluping have variable $\varepsilon_{Nd}(t)$ values (−4.89–4.98; Table 2) and T_{DM} model ages (2.32–2.95 Ga; Table 2). The highest $\varepsilon_{Nd}(t)$ value (4.98) lies on the depleted mantle curve (Fig. 10a), and the youngest T_{DM} model age (2.32 Ga) is similar to the crystallization age of the Tieluping TTG (2318 ± 8 Ma). The most negative $\varepsilon_{Nd}(t)$ value in the Tieluping gneisses corresponds to the oldest T_{DM} model age (2.95 Ga), similar to the amphibolites (Table 2). The Taihua Complex at Lushan was originally derived from depleted mantle at 2.8–3.1 Ga (Huang et al., 2010), and there is a Sm–Nd isotopic fractionation trend from mafic to felsic rocks at about 3.0 Ga (Fig. 10b). The Taihua gneisses at Xiong'er mostly depart from this trend except for some Tieluping samples. Overall, the Taihua Complex at Xiong'er shows a mixing trend between juvenile melts and old crustal materials (Fig. 10b), and was likely originally derived from an overall younger reservoir than that at Lushan (Fig. 10b).

5. Discussion

5.1. Petrogenesis of the Taihua TTG gneisses in the Xiong'er area

5.1.1. High Sr/Y and La/Yb

The high Sr/Y and La/Yb ratios are typical features of TTGs and adakites (Martin et al., 2005) and are attributed either to melting of a high Sr/Y source (Moyen, 2009), with different contributions of plagioclase, amphibole or garnet during melting (e.g., Drummond and Defant, 1990; Martin et al., 2005; Moyen, 2009) or fractional crystallization (Huang et al., 2010; Macpherson et al., 2006). Since Early Neoarchean TTGs occur in the Lushan area (Huang et al., 2010), melting of a high Sr/Y and La/Yb source is possible to explain the features of the Paleoproterozoic Xiong'er TTGs. However, this mechanism is unlikely to be sufficient for their genesis because of highly variable Sr/Y, La/Yb, HREE and Y in the Tieluping TTG gneisses (Figs. 8 and

Table 2
Nd isotope compositions of the Taihua gneisses and amphibolites in the Xiong'er area.

Samples	Rocks	$^{147}Sm/^{144}Nd$ [a]	$^{143}Nd/^{144}Nd(\pm2\sigma)$	$(^{143}Nd/^{144}Nd)_i$	$\varepsilon_{Nd}(t)$ [b]	$f_{Sm/Nd}$ [c]	T_{DM}(Ma) [d]	T_{DM2}(Ma) [e]
Ganshugou								
THX05-40	Tonalite gneiss	0.1167	0.511377 ± 7	0.509778	−3.25	−0.41	2775	2784
THX05-41	Tonalite gneiss	0.0996	0.511081 ± 8	0.509717	−4.45	−0.49	2751	2880
THX08-29	Tonalite gneiss	0.0862	0.511006 ± 7	0.509825	−2.33	−0.56	2553	2711
THX05-44	Kfs granite gneiss	0.0990	0.511045 ± 7	0.509689	−5.01	−0.50	2785	2926
THX05-45	Kfs granite gneiss	0.1127	0.511277 ± 7	0.509734	−4.12	−0.43	2813	2854
THX05-42	Amphibolite	0.1488	0.511893 ± 7	0.509262	2.00	−0.24	2941	2857
THX08-39	Amphibolite	0.1337	0.511634 ± 6	0.509269	2.14	−0.32	2877	2845
Tieluping								
THX05-49	Tonalite gneiss	0.0946	0.510912 ± 11	0.509465	−3.24	−0.52	2851	2981
THX05-53	Tonalite gneiss	0.0928	0.510800 ± 6	0.509382	−4.89	−0.53	2947	3112
THX08-51	Granodiorite gneiss	0.0827	0.510830 ± 8	0.509566	−1.28	−0.58	2687	2823
THX08-54	Diorite gneiss	0.1089	0.511125 ± 11	0.509459	−3.36	−0.45	2932	2990
THX08-55	Tonalite gneiss	0.0994	0.511008 ± 7	0.509488	−2.80	−0.49	2843	2945
THX08-57	Granodiorite gneiss	0.1009	0.511427 ± 11	0.509885	4.98	−0.49	2321	2321
THX08-59	Granodiorite gneiss	0.0708	0.510872 ± 9	0.509790	3.12	−0.64	2421	2470
Sh-4 [f]	Gneiss	0.1169	0.511312 ± 5	0.509525	−2.07	−0.41	2880	2886
Sh-6 [f]	Gneiss	0.1103	0.511165 ± 13	0.509478	−3.00	−0.44	2913	2961
Sh-9 [f]	Gneiss	0.0971	0.510991 ± 8	0.509506	−2.45	−0.51	2810	2917
Sh-5 [f]	Amphibolite	0.1168	0.511284 ± 14	0.509218	1.14	−0.41	2922	2925

[a] Calculated by using whole-rock Sm and Nd contents.
[b] $\varepsilon_{Nd}(t) = [(^{143}Nd/^{144}Nd)_S/(^{143}Nd/^{144}Nd)_{CHUR} - 1] \times 10000$; t = 2.32 Ga (Tieluping gneiss), 2.07 Ga (Ganshugou gneiss), 2.68 Ga (amphibolite; Ni et al., 2003).
[c] $f_{Sm/Nd} = [(^{147}Sm/^{144}Nd)_S/(^{147}Sm/^{144}Nd)_{CHUR}] - 1$ (Shirey and Hanson, 1986).
[d] $T_{DM} = \ln\{[(^{143}Nd/^{144}Nd)_s - (^{143}Nd/^{144}Nd)_{DM}]/[(^{143}Sm/^{144}Nd)_s - (^{147}Sm/^{144}Nd)_{DM}]\}/\lambda$ (DePaolo, 1981).
[e] $T_{DM2} = T_{DM1} - (T_{DM1} - t)((f_{cc} - f_S)/(f_{cc} - f_{DM}))$ (Keto and Jacobsen, 1987); where S = sample, f_{cc}, f_S and f_{DM} are $f_{Sm/Nd}$ values of the average continental crust, the sample and the depleted mantle, respectively. In the calculation, $(^{143}Nd/^{144}Nd)_{CHUR} = 0.512638$, $(^{147}Sm/^{144}Nd)_{CHUR} = 0.1967$, $(^{143}Nd/^{144}Nd)_{DM} = 0.51315$, $(^{147}Sm/^{144}Nd)_{DM} = 0.2136$, $f_{cc} = -0.4$, $f_{DM} = 0.08592$.
[f] Data from Zhang and Li (1998).

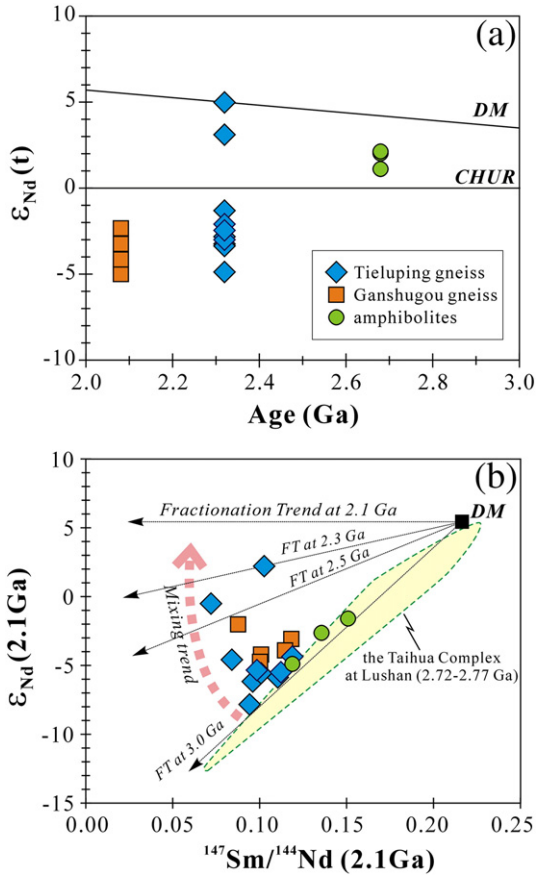

Fig. 10. Nd isotopic evolution diagrams for the Xiong'er–Taihua gneisses and amphibolites: (a) $\varepsilon_{Nd}(t)$ vs. ages; (b) ε_{Nd} vs. $^{147}Sm/^{144}Nd$ at 2.1 Ga. The Taihua Complex at Lushan (Huang et al., 2010) is shown as representing typical Late Archean rocks in the southern North China Craton for comparison. Three gneiss samples and one amphibolite sample from Tieluping (Table 2) were selected from Zhang and Li (1998).

9). Additionally, high $Mg^{\#}$ (0.42–0.53; Table 1) or very high Sr/Y ratios (up to 220) are inconsistent with partial melting of a high Sr/Y source (usually medium Sr/Y and low $Mg^{\#}$; Moyen, 2009). Thus various contributions of plagioclase, amphibole or garnet during melting or fractional crystallization would likely be the main mechanism for the high Sr/Y and La/Yb characteristics of the Tieluping TTG gneisses.

It is always difficult to distinguish whether garnet and amphibole acted as residual phases during partial melting or as fractionating phases because both processes can produce high Sr/Y and La/Yb ratios in the TTG melts. As in the partial melting model of Drummond and Defant (1990), relatively low degree partial melting (<30%) with an amphibolite or eclogite restite would be required to explain the high Sr/Y and La/Yb (Fig. 9). However, partial melting of less than 30% would not produce large variations in the Y and Yb contents within a rock suite (Figs. 9 and 11a). Thus the great variation of Y and Yb contents in the Tieluping TTG gneisses is inconsistent with a partial melting model, and the fractional crystallization of garnet and/or amphibole is more likely to have produced the high Sr/Y and La/Yb ratios in these gneisses (Fig. 11a). Furthermore, amphibole has a high K_D for HREEs, but even higher for medium REEs (e.g., Dy); therefore, amphibole removal can result in decreasing Dy/Yb ratios. The separation of garnet will not only effectively raise the Sr/Y and La/Yb ratios, but also increase the Dy/Yb ratio in the melt (Davidson et al., 2007; Huang et al., 2010; Macpherson et al., 2006). The variable Dy/Yb ratios (1.79–3.83; Table 1) in the Tieluping TTG gneisses are positively correlated to Sr/Y and $[La/Yb]_N$ (Fig. 11b, c), thus corresponding to garnet fractionation. High Dy/Yb ratios in some Tieluping samples indicate that garnet fractionation could be an important mechanism for the high Sr/Y and La/Yb in the Taihua TTG gneisses at Xiong'er. For the samples with high SiO_2 (>65 wt.%), Al_2O_3 decreases with increasing SiO_2 (Fig. 6e), compatible with the fractionation of Al-rich minerals such as garnet.

The Tieluping TTG gneisses show variable major oxide contents, including SiO_2, MgO, Fe_2O_3 and CaO (Fig. 6), thus the fractionation of amphibole and/or clinopyroxene is also important, although amphibole fractionation is preferred for the following reason. The separation of garnet would produce distinctive drops from medium to heavy REEs on the REE patterns of the melts. The highly fractionated samples (e.g., THX08-51 and THX08-59) have relatively flat HREE patterns (Fig. 8c), suggesting the buffering effect of amphibole fractionation, while clinopyroxene fractionation could not be responsible for such an effect.

Both samples THX08-51 and THX08-59 are characterized by very high $[La/Yb]_N$ ratios (Figs. 9a, 11c, d). Sample THX08-51 also has high Sr/Y, but sample THX08-59 has a low Sr/Y ratio (Fig. 11d). Both samples THX08-51 and THX08-59 are granodiorites with high SiO_2 (>70 wt.%; Table 1), indicating that they were derived from low-degree partial melting or underwent a high degree of fractional crystallization of amphibole and/or garnet (Fig. 11c, d), which might be responsible for their extraordinary high $[La/Yb]_N$ ratios. Removal (or accumulation) of plagioclase would be effective in reducing (or increasing) Sr, Sr/Y and Eu/Eu*, but would have less effect on La/Yb and will not affect Dy/Yb in the melts (Huang et al., 2010). Thus sample THX08-59 was probably formed by removal of plagioclase (Fig. 11d), compatible with its negative Eu and Sr anomalies (Fig. 8). However, high Sr/Y and $[La/Yb]_N$ ratios in THX08-51 cannot be attributed to plagioclase accumulation because of very weak positive Eu and Sr anomalies (Fig. 8), similar to the results of high degree fractionation of garnet + amphibole (Fig. 11). On the contrary, sample THX05-55 has relatively low Dy/Yb and $[La/Yb]_N$ ratios (1.79 and 16.5, respectively; Table 1), moderate Sr/Y (50.0; Table 1) but high Eu/Eu* (1.14; Table 1) and Sr (512 ppm; Table 1), corresponding to slight accumulation of plagioclase. Although the positive (or negative) correlations between Sr/Y (and $[La/Yb]_N$) and MgO or SiO_2 would be expected by the fractionation model (Macpherson et al., 2006), this estimation is not suitable for the Tieluping TTGs because of the buffering effect of plagioclase accumulation or fractionation in some samples.

By comparison, the Muce TTG gneisses show constant Sr/Y and $[La/Yb]_N$ (Figs. 9, 11) relative to variable SiO_2 and MgO (Fig. 6), which might favor the partial melting model, and the contribution of garnet fractionation is apparently weak (Fig. 11). The relatively low and constant Dy/Yb ratios of the Muce TTG gneisses also indicate that garnet is really not significant in the genesis of the Muce TTG gneisses. On the other hand, the variable major element contents (e.g., SiO_2, MgO, Fe_2O_3 and CaO; Fig. 6) but overall high $Mg^{\#}$ values (46.8–50.1; Diwu et al., 2007) of the Muce TTG gneisses are likely due to fractional crystallization of amphibole. The Muce TTG gneisses all show depleted and concave-upward REE patterns between middle and heavy REEs (Fig. 8), corresponding to the effect of amphibole extraction, because amphibole has a high partition coefficient for these elements.

Some Tieluping and all Muce TTG gneisses have relatively low $[La/Yb]_N$, Sr/Y and Dy/Yb ratios but high Y and Yb contents, suggesting amphibole was the dominant residual phase during partial melting (Figs. 9, 11). Most post-Archean TTGs show a fractional crystallization sequence extending from diorite to granite (Condie, 2005). The Taihua TTG gneisses at Xiong'er also have wide compositional ranges consistent with the extensive fractional crystallization of garnet + amphibole at Tieluping, but dominantly amphibole at Muce.

5.1.2. Source characteristics and petrogenesis

Both the Tieluping and Muce TTG gneisses have high $Mg^{\#}$ (Fig. 12a), thus an overall mafic source is proposed. Additionally, the $Mg^{\#}$ values of most Tieluping and all Muce TTG gneisses are even higher than the experimental melts of natural hydrous basalts

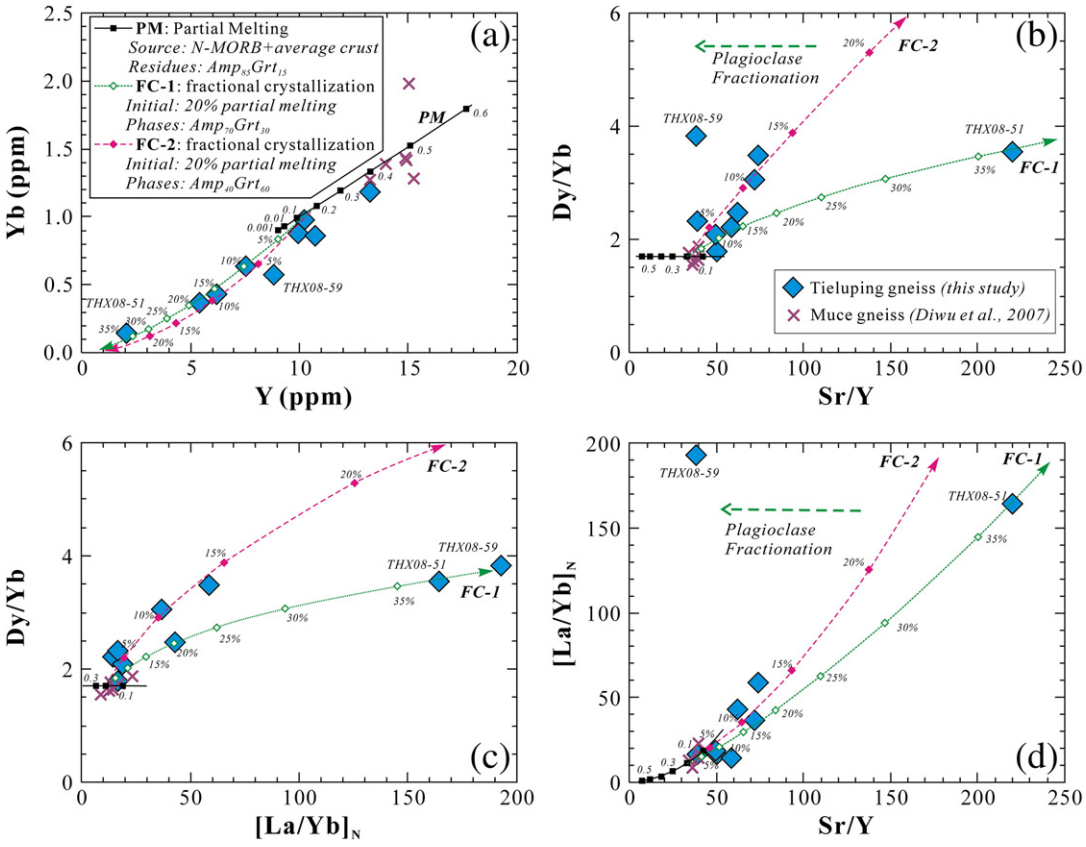

Fig. 11. Diagrams showing relationships of (a) Yb vs. Y, (b) Dy/Yb vs. Sr/Y, (c) Dy/Yb vs. $[La/Yb]_N$ and (d) $[La/Yb]_N$ v.s. Sr/Y for the Taihua TTG gneisses in the Xiong'er area. Partial melting curves (PM) and Rayleigh fractional crystallization curves (FC-1, FC-2) were calculated by using partition coefficients in the system of andesitic to tonalitic melts: amphibole (Sisson, 1994), garnet (Barth et al., 2002), plagioclase (Drake and Weill, 1975). The N-MORB average is from Hofmann (1988), and the average crust is from Rudnick and Gao (2003).

at 1–4 GPa (Fig. 12a), which indicates that initial TTG melts would have interacted with mafic melts from the mantle. High $Mg^{\#}$ in adakites is due to interaction between slab-melt and mantle peridotite during ascent through the mantle wedge (e.g., Martin et al., 2005; Rapp et al., 1999). Thus subducting ocean crust under eclogite facies conditions would be the potential source material for TTGs as an analog of adakite (e.g., Defant and Drummond, 1990; Martin et al., 2005). However, this process can also significantly modify Ni and Cr contents in the final melts (Fig. 12b, c) without changing the slab-melt signature as recorded by REE, Sr and Y (e.g., Martin et al., 2005; Rapp et al., 1999; Smithies, 2000). Both the Tieluping and Muce TTG gneisses have low Cr and Ni contents and plot in the fields of thick lower crust-derived adakitic rocks (Fig. 12b, c, d), indicating that the Taihua TTG gneisses at Xiong'er could not be derived from subducting oceanic lithosphere with slab-melts that had reacted with peridotitic mantle. In addition, typical slab melts generally have low Rb/Sr ratios (<0.05), in contrast to the wide range of Rb/Sr ratios (0.01–0.4) for adakites derived from thickened crust (Huang et al., 2009). The Taihua TTG gneisses at Xiong'er have high Rb/Sr ratios (0.07–0.33; Table 1), thereby arguing against slab melting and indicating a large contribution from the lower crust in their generation.

Most early Archean and many late Archean TTG suites likely represent partial melts of basaltic lower crust rather than subducted/subducting ocean crust (Condie, 2005; Smithies, 2000; Smithies and Champion, 2000) because there is little opportunity for Archean slab melts to react with the mantle wedge (Condie, 2005; Huang et al., 2010). The Taihua TTGs in the southern segment of the TNCO are also likely partial melts of basaltic lower crust because of overall low whole rock $\varepsilon_{Nd}(t)$ and zircon $\varepsilon_{Hf}(t)$ values (Figs. 5 and 10). Additionally, the Tieluping diorite sample (THX08-54) contains inherited zircons with ages of 2496 ± 4 Ma to 3352 ± 14 Ma, also suggesting the participation of pre-existing crustal materials. On the other hand, some Tieluping TTG gneisses have positive $\varepsilon_{Nd}(t)$ values, and the youngest Nd model age of 2.32 Ga is very close to the crystallization age of 2318 ± 8 Ma, indicating the extensive participation of juvenile components in the source. The juvenile components were basaltic materials from the mantle according to the high $Mg^{\#}$ values of most Tieluping and all Muce TTG gneisses, which could possibly be related to mafic magma underplating. The underplating of basaltic magmas would not only thicken the crust and add juvenile components to lower crust, but also trigger the partial melting of pre-existing lower crustal materials.

5.2. Petrogenesis of the Ganshugou potassium-rich gneisses

Zircon U–Pb dating reveals at least two episodes of magmatism (~2.20 Ga and 2.08 Ga, respectively; Fig. 4) in the gneisses from Ganshugou, which are therefore more complex than the Tieluping and Muce TTG gneisses (Fig. 4). However, all the Ganshugou gneisses are similar in having high potassium contents and belonging to the high-K calc-alkaline or shoshonitic series (Fig. 6h), quite different from the Tieluping and Muce TTG gneisses that have high Al_2O, CaO and Na_2O (Fig. 6e, f, g) but low K_2O (Fig. 6h). Furthermore, the low SiO_2 samples (SiO_2<60 wt.%, such as THX08-29, THX08-35 and THX05-41; Table 1) are all members of the shoshonitic series, indicating initially high-potassium melts.

There are several tectonic settings for the generation of potassic igneous rocks: continental arc, post-collisional arc, oceanic arc and within-plate (Müller and Groves, 1997; Müller et al., 1992). The within-plate potassic igneous rocks are associated with hot-spot activity or with extensional (particularly rift) tectonics (Müller and Groves, 1997), which are inconsistent with the Ganshugou gneisses characterized by weakly negative whole-rock $\varepsilon_{Nd}(t)$ (−5.01 to

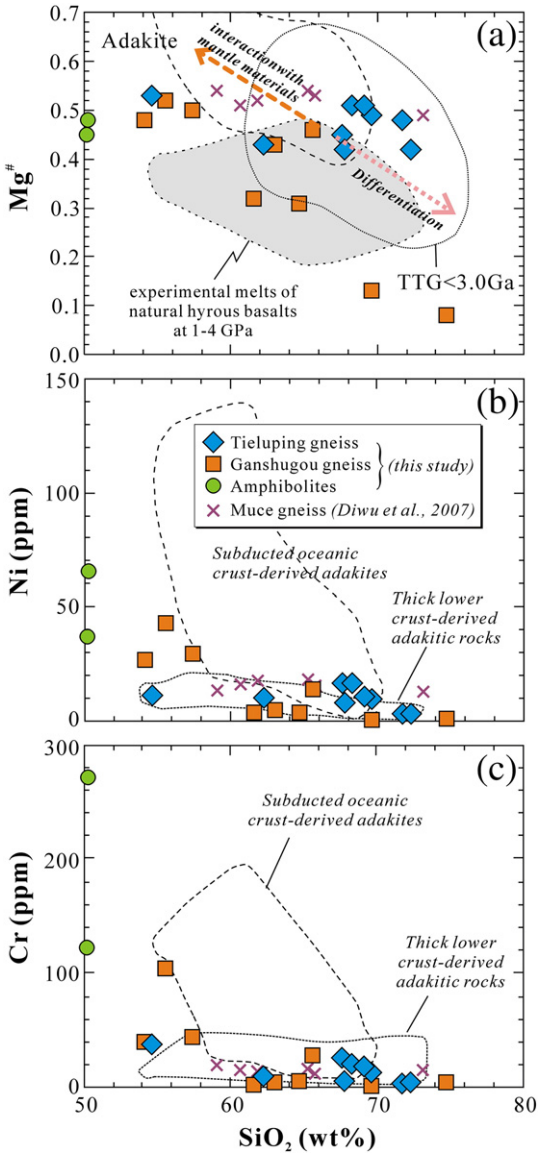

Fig. 12. Diagrams of (a) $Mg^{\#}$ vs. SiO_2, (b) Ni vs. SiO_2 and (c) Cr vs. SiO_2 for the Taihua gneisses and amphibolites in the Xiong'er area. $Mg^{\#}$ fields of adakite and TTG are after the compilations of Smithies (2000), and the Cr and Ni fields of adakites are after the compilation of Wang et al. (2006).

−2.33; Table 2) and zircon $\varepsilon_{Hf}(t)$ values (Fig. 5a, b) and Ta–Nb–Ti depletions (Fig. 8). The Ganshugou gneisses also differ from oceanic arc potassic igneous rocks which are generally low in HFSE (e.g. Zr<300 ppm; Nb<20 ppm; Hf<5 ppm; Müller and Groves, 1997). In terms of radiogenic whole-rock Nd isotopes (Fig. 10), zircon Hf isotopes (Fig. 5a, b) and Ta–Nb–Ti depletions (Fig. 8), the Ganshugou gneisses are more like continental or post-collisional potassic igneous rocks. There is a progressive transition to more alkaline magmatism in post-collisional arcs, and continental arc potassic igneous rocks have slightly higher Rb, Sr, Ba and Ce, but lower Nb and P contents than the post-collisional rocks (Müller and Groves, 1997). The potassium-rich gneisses from Ganshugou contain elevated Nb concentrations (up to 26.7 ppm; Table 1) without positive Sr anomalies (Fig. 8b), features consistent with potassic igneous rocks from a post-collisional arc setting (Müller and Groves, 1997).

The large discrepancies between crystallization ages (2.07–2.19 Ga) and the whole rock T_{DM} model ages (2.81–2.55 Ga) and T_{DM2} model ages (2.71–2.93 Ga) of the Ganshugou gneisses (Table 2) require the participation of recycled continental crustal materials. Additionally, the heterogeneous zircon $\varepsilon_{Hf}(t)$ values (Fig. 5; Table 2) in the Ganshugou gneisses, corresponding to old zircon $T_{DM\text{-}Hf}$ and $T^{C}_{DM\text{-}Hf}$ model ages (Supplemental Table 3), also confirm a source dominated by older recycled continental crustal materials. The zircon "crustal" Hf model ages of the Ganshugou gneisses (2.64–3.23 Ga, mean value 3.10±0.03 Ga) are much older than the whole-rock Nd model ages (2.55–2.81 Ga, mean value 2.74±0.10 Ga), which may be related to the modification of Nd isotopes during crustal accretion and the preservation of initial $\varepsilon_{Hf}(t)$ values in zircons owing to their resistance to alteration. In contrast to the Tieluping and Muce TTG gneisses, the Ganshugou potassium-rich gneisses all show negative europium anomalies and relatively high HREE, indicating that the Ganshugou potassium-rich magma was formed at relatively shallow crustal depths with plagioclase, rather than garnet or amphibole, as a residual or fractionating phase. A shallow source is also compatible with the post-collisional arc setting which is characterized by complex magmatic activity and tectonic uplift (Müller et al., 1992; Wilson, 1989). Additionally, both zircon Hf and whole rock Nd model ages of the Ganshugou gneisses are older than those of Tieluping and Muce TTG gneisses (Figs. 5, 10; Tables 2), suggesting that the Ganshugou potassium-rich rocks were derived from an overall older reservoir than those of the Tieluping TTG, which is consistent with more juvenile components in the latter due to mafic magma underplating at 2.30–2.32 Ga.

5.3. Implications for tectonic transformation in the southern segment of the TNCO in the Early Paleoproterozoic

Based on Sm–Nd isochrons, depleted mantle Nd model ages and single-grain zircon evaporation Pb–Pb ages, it was previously suggested that the Taihua Complex in the Xiong'er area is similar to that in the Lushan area, and that it was formed during Neoarchean time and underwent metamorphism in the Paleoproterozoic (Guan, 1996; Ni et al., 2003; Zhang and Li, 1998). However, the zircon ages from the Ganshugou potassium-rich gneisses (SHRIMP: 2065±23 Ma to 2188±26 Ma), Tieluping TTG gneisses (CAMECA 1280: 2305±23 Ma to 2318±8 Ma) and Muce TTGs (LA-ICP-MS: 2316±16 Ma to 2336±13 Ma; Diwu et al., 2007) reveal that the Taihua Complex in the Xiong'er area was formed mainly during Early Paleoproterozoic time, much later than that in the Lushan area.

The Taihua TTG at Xiong'er was formed through extensive fractional crystallization of garnet+amphibole and/or with garnet +amphibole as residual phases in the source, suggesting thickening of the crust in the southern segment of TNCO at 2.30–2.32 Ga. This might have resulted from several processes, such as orogenesis (e.g., Burg and Ford, 1997), repeated underplating (e.g., Furlong and Fountain, 1986; Haschke et al., 2002), intra-oceanic plate stacking (De Wit, 1998) and/or oceanic plateau accretion (e.g., Condie, 1997; De Wit et al., 1992; Desrochers et al., 1993). The last two processes are not applicable for genesis of the Taihua TTGs at Xiong'er because inherited zircons (2286±7 Ma to 3352±14 Ma), whole rock $\varepsilon_{Nd}(t)$ and zircon $\varepsilon_{Hf}(t)$ values all suggest the participation of pre-existing crustal materials. Probably the most effective thickening process is tectonic shortening at the convergence zone between two plates (Giese et al., 1999). In the southern TNCO, it was possible that the Early Paleoproterozoic collision between micro-continents occurred after Neoarchean slab-subduction, which is similar to modern orogenic belts and does not exclude the underplating of basaltic rocks. Based on the geochronology and petrology of the Lüliang Complex in the central part of the TNCO, Zhao et al. (2008) proposed that the TNCO may represent a long-lived magmatic arc (>650 Ma). The TTG gneisses from the Taihua Complex in southern segment of the TNCO formed from a combination of pre-existing continental crust and juvenile materials, implying an Andean-type continental margin arc environment and subsequent accretionary orogenesis. This indicates that the TNCO had experienced subduction in the Early Paleoproterozoic, which would be an evidence of long-lived magmatic

arc before the collision between the Eastern and Western Blocks to form the North China Craton (Zhao et al., 2008).

The Taihua Complex in the southern segment of the TNCO shows a compositional change in the Early Paleoproterozoic: at 2.30–2.32 Ga, the Tieluping and Muce TTG gneisses are mostly low-K, whereas at 2.07–2.19 Ga, the Ganshugou gneisses are all potassium-rich intermediate to felsic rocks (Fig. 6h; Table 1). The preferred setting to generate the Ganshugou potassic-rich rocks is a post-collisional setting, characterized by tectonic uplift after the collision of continental plates, at which the suture zone forms an area of crustal thickening following ocean-basin closure (Müller et al., 1992; Wilson, 1989). Thus, the temporal change from mostly low-K igneous rocks (TTG) to mostly high-K igneous rocks in the southern segment of the TNCO indicates the tectonic transformation from accretionary orogenesis (2.30–2.32 Ga) to extensional regimes (2.08–2.19 Ga) as a consequence of post-collisional uplift in the Early Paleoproterozoic.

6. Conclusions

On the basis of geochronological, geochemical and Nd–Hf isotopic data, the following conclusions can be drawn regarding the origin and tectonic setting of the Taihua Complex in the southern segment of the TNCO:

(1) Zircon U–Pb dating indicates that the Taihua Complex in the Xiong'er area formed mainly in the Early Paleoproterozoic, and includes an early TTG suite (~2.30–2.32 Ga) and a later potassium-rich granitoid suite (2.07–2.19 Ga).
(2) The Tieluping TTG rocks were most likely derived by partial melting of thickened lower crust and underwent garnet ± amphibole fractionation, together with plagioclase accumulation and/or fractionation. In comparison, the Ganshugou potassium-rich rocks were the result of partial melting of pre-existing crustal materials at relatively shallow depths.
(3) Crustal thickening is attributed to accretionary orogenesis accompanied by basaltic underplating, with the potassium-rich rocks generated in a post-collisional setting. There is thus a tectonic transformation in the southern TNCO from orogenic collision to an extensional regime as a consequence of post-collisional uplift in the Early Paleoproterozoic.

Supplementary materials related to this article can be found online at doi:10.1016/j.lithos.2012.01.004.

Acknowledgements

We gratefully acknowledge the careful and constructive comments of G.C. Zhao and F. Pirajno, who helped considerably in improving the manuscript. We also thank Q.L. Li for CAMECA U–Pb zircon dating, B. Song for SHRIMP U–Pb zircon dating, Y.H. Yang for zircon Lu–Hf isotope analyses, Y. Liu for major element analyses, X.L. Tu for trace element analyses and X.R. Liang for Nd isotope analyses. This research was supported by the Knowledge Innovation Project of the Chinese Academy of Sciences (KZCX2-YW-QN106, KZCX2-YW-Q08-3-6), National Natural Science Foundation of China (NSFC Projects 40573015, 90714001) and the CAS/SAFEA International Partnership Program for Creative Research Teams (KZCX2-YW-Q04-06). This is contribution No. IS-1434 from GIGCAS and TIGeR publication number 397.

References

Barker, F., Arth, J.G., 1976. Generation of trondhjemitic–tonalitic liquids and Archaean bimodal trondhjemite–basalt suites. Geology 4, 596–600.
Barth, M.G., Foley, S.F., Horn, I., 2002. Partial melting in Archean subduction zones: constraints from experimentally determined trace element partition coefficients between eclogitic minerals and tonalitic melts under upper mantle conditions. Precambrian Research 113, 323–340.
BGMR (Bureau of Geology and Mineral Resources), 1965. Geological map of Henan Province. Sheet I-49-XVI (Luoning) scale 1 : 200,000. Zhengzhou.
Burg, J.-P., Ford, M., 1997. Orogeny through time: an overview. Geological Society of London. Special Publication 121, 1–17.
Condie, K.C., 1997. Contrasting sources for upper and lower continental crust: the greenstone connection. Journal of Geology 105, 729–736.
Condie, K.C., 2000. Episodic continental growth models: afterthoughts and extensions. Tectonophysics 322, 153–162.
Condie, K.C., 2005. TTGs and adakites: are they both slab melts? Lithos 80, 33–44.
Condie, K.C., O'Neill, C., Aster, R.C., 2009. Evidence and implications for a widespread magmatic shutdown for 250 My on earth. Earth and Planetary Science Letters 282, 294–298.
Davidson, J., Macpherson, C., Turner, S., 2007. Amphibole control in the differentiation of arc magmas. Geochimica et Cosmochimica Acta 71, A204.
De Wit, M.J., 1998. On Archean granites, greenstones, cratons and tectonics: does the evidence demand a verdict? Precambrian Research 91, 181–226.
De Wit, M.J., Roering, C., Hart, R.J., Armstrong, R.A., de Ronde, C.E.J., Green, R.W.E., Tredoux, M., Peberdy, E., Hart, R.A., 1992. Formation of an Archaean continent. Nature 357, 553–562.
Defant, M.J., Drummond, M.S., 1990. Derivation of some modern arc magmas by melting of young subducted lithosphere. Nature 347, 662–665.
DePaolo, D.J., 1981. A neodymium and strontium isotopic study of the Mesozoic calc-alkaline granitic batholiths of the Sierra Nevada and Peninsular Ranges, California. Journal of Geophysical Research 86, 10470–10488.
Desrochers, J.P., Hubert, C., Ludden, J., Pilote, P., 1993. Accretion of Archean oceanic plateau fragments in the Abitibi greenstone belt, Canada. Geology 21, 451–454.
Diwu, C.R., Sun, Y., Lin, C.L., Liu, X.M., Wang, H.L., 2007. Zircon U–Pb ages and Hf isotopes and their geological significance of Yiyang TTG gneisses from Henan province, China. Acta Petrologica Sinica 23, 253–262 (in Chinese with English abstract).
Drake, M.J., Weill, D.F., 1975. Partition of Sr, Ba, Ca, Y, Eu^{2+}, Eu^{3+} and other REE between plagioclase feldspar and magmatic liquid: an experimental study. Geochimica et Cosmochimica Acta 39, 689–712.
Drummond, M.S., Defant, M.J., 1990. A model for trondhjemite–tonalite–dacite genesis and crustal growth via slab melting: Archean to modern comparisons. Journal of Geophysical Research 95, 21503–21521.
Furlong, K.P., Fountain, D.M., 1986. Continental crustal underplating: thermal considerations and seismic–petrologic consequences. Journal of Geophysical Research 91, 8285–8294.
Giese, P., Scheuber, E., Schilling, F., Schmitz, M., Wigger, P., 1999. Crustal thickening processes in the Central Andes and the different natures of the Moho-discontinuity. Journal of South American Earth Sciences 12, 201–220.
Griffin, W.L., Pearson, N.J., Belousova, E., Jackson, S.E., O'Reilly, S.Y., van Achterberg, E., Shee, S.R., 2000. The Hf isotope composition of cratonic mantle: LAM-MC-ICPMS analysis of zircon megacrysts in kimberlites. Geochimica et Cosmochimica Acta 64, 133–147.
Griffin, W.L., Belousova, E.A., Shee, S.R., Pearson, N.J., O'Reilly, S.Y., 2004. Archean crustal evolution in the northern Yilgarn Craton: U–Pb and Hf-isotope evidence from detrital zircons. Precambrian Research 131, 231–282.
Griffin, W.L., Pearson, N.J., Belousova, E.A., Saeed, A., 2006. Comment: Hf-isotope heterogeneity in zircon 91500. Chemical Geology 233, 358–363.
Guan, B.D. (Ed.), 1996. The Precambrian–Lower Cambrian Geology and Metallogenesis in the South Border of the North China Platform in Henan Province. Press of China University of Geosciences, Wuhan, pp. 1–328.
Guo, J.H., Sun, M., Zhai, M.G., 2005. Sm–Nd and SHRIMP U–Pb zircon geochronology of high-pressure granulites in the Sanggan area, North China Craton: timing of Paleoproterozoic continental collision. Journal of Asian Earth Sciences 24, 629–642.
Haschke, M., Siebel, W., Günther, A., Scheuber, E., 2002. Repeated crustal thickening and recycling during the Andean Orogeny in north Chile (21°–26°S). Journal of Geophysical Research 107, 2019. doi:10.1029/2001JB000328.
He, Y.H., Zhao, G.C., Sun, M., Xia, X.P., 2009. SHRIMP and LA-ICP-MS zircon geochronology of the Xiong'er volcanic rocks: implications for the Paleo-Mesoproterozoic evolution of the southern margin of the North China Craton. Precambrian Research 168, 213–222.
Hofmann, A.W., 1988. Chemical differentiation of the earth: the relationship between mantle, continental crust, and oceanic crust. Earth and Planetary Science Letters 90, 297–314.
Huang, X.L., Xu, Y.G., Lan, J.B., Yang, Q.J., Luo, Z.Y., 2009. Neoproterozoic adakitic rocks from Mopanshan in the western Yangtze Craton: partial melts of a thickened lower crust. Lithos 112, 367–381.
Huang, X.L., Niu, Y.L., Xu, Y.G., Yang, Q.J., Zhong, J.W., 2010. Geochemistry of TTG and TTG-like gneisses from Lushan–Taihua complex in the southern North China Craton: implications for late Archean crustal accretion. Precambrian Research 182, 43–56.
Kemp, A.I.S., Hawkesworth, C.J., Paterson, B.A., Kinny, P.D., 2006. Episodic growth of the Gondwana supercontinent from hafnium and oxygen isotopes in zircon. Nature 439, 580–583.
Keto, L.S., Jacobsen, S.B., 1987. Nd and Sr isotopic variations of Early Paleozoic oceans. Earth and Planetary Science Letters 84, 27–41.
Li, X.H., Li, Z.X., Wingate, M.T.D., Chung, S.L., Liu, Y., Lin, G.C., Li, W.X., 2006. Geochemistry of the 755 Ma Mundine Well dyke swarm, northwestern Australia: part of a Neoproterozoic mantle superplume beneath Rodinia? Precambrian Research 146, 1–15.
Li, X.H., Liu, Y., Li, Q.L., Guo, C.H., Chamberlain, K.R., 2009. Precise determination of Phanerozoic zircon Pb/Pb age by multicollector SIMS without external standardization. Geochemistry, Geophysics, Geosystems 10, Q04010. doi:10.1029/2009GC002400.
Liu, D.Y., Nutman, A.P., Compston, W., Wu, J.S., Shen, Q.H., 1992. Remnants of 3800 Ma crust in the Chinese Part of the Sino-Korean craton. Geology 20, 339–342.

Liu, S.W., Zhao, G.C., Wilde, S.A., Shu, G.M., Sun, M., Li, Q.G., Tian, W., Zhang, J., 2006. Th–U–Pb monazite geochronology of the Lüliang and Wutai complexes: constraints on the tectonothermal evolution of the Trans-North China Orogen. Precambrian Research 148, 205–225.

Liu, D.Y., Wilde, S.A., Wan, Y.S., Wang, S.Y., Valley, J.W., Kita, N., Dong, C.Y., Xie, H.Q., Yang, C.X., Zhang, Y.X., Gao, L.Z., 2009. Combined U–Pb, hafnium and oxygen isotope analysis of zircons from meta-igneous rocks in the southern North China Craton reveal multiple events in the Late-Mesoarchean–Early Neoarchean. Chemical Geology 261, 140–154.

Ludwig, K.R., 2003. Isopot: a geochronological toolkit for Microsoft Excel. Berkeley Geochronology Centre Special Publication, 4, pp. 1–67.

Macpherson, C.G., Dreher, S., Thirlwall, M.F., 2006. Adakites without slab melting: High pressure differentiation of island arc magma, Mindanao, the Philippines. Earth and Planetary Science Letters 243, 581–593.

Martin, H., Smithies, R.H., Rapp, R., Moyen, J.F., Champion, D., 2005. An overview of adakite, tonalite–trondhjemite–granodiorite (TTG), and sanukitoid: relationships and some implications for crustal evolution. Lithos 79, 1–24.

Moyen, J.-F., 2009. High Sr/Y and La/Yb ratios: the meaning of the "adakitic signature". Lithos 112, 556–574.

Müller, D., Groves, D.I. (Eds.), 1997. Potassic Igneous Rocks and Associated Gold-Copper Mineralization. Springer-Verlag, Berlin Heidelberg, pp. 1–225.

Müller, D., Rock, N.M.S., Groves, D.I., 1992. Geochemical discrimination between shoshonitic and potassic volcanic rocks from different tectonic settings: a pilot study. Mineralogy and Petrology 46, 259–289.

Ni, Z.Y., Wang, R.M., Tong, Y., Yang, C., Dai, T.M., 2003. $^{207}Pb/^{206}Pb$ age of zircon and $^{40}Ar/^{39}Ar$ of amphibole from plagioclase amphibolite in the Taihua Group, Luoning, Henan, China. Geological Review 49, 361–366 (in Chinese with English abstract).

Rapp, R.P., Shimizu, N., Norman, M.D., Applegate, G.S., 1999. Reaction between slab-derived melts and peridotite in the mantle wedge: experimental constraints at 3.8 GPa. Chemical Geology 160, 335–356.

Rudnick, R.L., Gao, S., 2003. The composition of the continental crust. In: Rudnick, R.L. (Ed.), The Crust. : Treatise on Geochemistry, vol. 3. Elsevier, Oxford, pp. 1–64.

Shirey, S.B., Hanson, G.N., 1986. Mantle heterogeneity and crustal recycling in Archean granite-greenstone belts: evidence from Nd isotopes and trace elements in the Rainy Lake area, Superior Province, Ontario, Canada. Geochimica et Cosmochimica Acta 50, 2631–2651.

Sisson, T.W., 1994. Hornblende-melt trace-element partitioning measured by ion microprobe. Chemical Geology 117, 331–344.

Smithies, R.H., 2000. The Archaean tonalite–trondhjemite–granodiorite (TTG) series is not an analogue of Cenozoic adakite. Earth and Planetary Science Letters 182, 115–125.

Smithies, R.H., Champion, D.C., 2000. The Archaean high-Mg diorite suite: links to tonalite–trondhjemite–granodiorite magmatism and implications for early Archaean crustal growth. Journal of Petrology 41, 1653–1671.

Sun, S.-S., McDonough, W.F., 1989. Chemical and isotopic systematics of oceanic basalts: implications for mantle composition and processes. In: Saunders, A.D., Norry, M.J. (Eds.), Magmatism in the Ocean Basins: Geological Society Special Publication, 42, pp. 313–345.

Taylor, S.R., McLennan, S.M., 1985. The Continental Crust: its Composition and Evolution. Blackwell, Oxford.

Wang, Q., Xu, J.F., Jian, P., Bao, Z.W., Zhao, Z.H., Li, C.F., Xiong, X.L., Ma, J.L., 2006. Petrogenesis of adakitic porphyries in an extensional tectonic setting, Dexing, South China: implications for the genesis of porphyry copper mineralization. Journal of Petrology 47, 119–144.

Wang, X.L., Jiang, S.Y., Dai, B.Z., 2010. Melting of enriched Archean subcontinental lithospheric mantle: evidence from the ca. 1760 Ma volcanic rocks of the Xiong'er Group, southern margin of the North China Craton. Precambrian Research 182, 204–216.

Wiedenbeck, M., Alle, P., Corfu, F., Griffin, W.L., Meier, M., Oberli, F., Vonquadt, A., Roddick, J.C., Speigel, W., 1995. 3 natural zircon standards for U–Th–Pb, Lu–Hf, trace-element and REE analyses. Geostandards Newsletter 19, 1–23.

Williams, I.S., 1998. U–Th–Pb geochronology by ion microprobe. In applications of microanalytical techniques to understanding mineralizing processes. Reviews in Economic Geology 7, 1–35.

Wilson, M., 1989. Igneous Petrogenesis: a Global Tectonic Approach. Unwin Hyman, London. 466 pp.

Wu, F.Y., Yang, Y.H., Xie, L.W., Yang, J.H., Xu, P., 2006. Hf isotopic compositions of the standard zircons and baddeleyites used in U–Pb geochronology. Chemical Geology 234, 105–126.

Xia, X.P., Sun, M., Zhao, G.C., Wu, F.Y., Xu, P., Zhang, J.H., Luo, Y., 2006. U–Pb and Hf isotopic study of detrital zircons from the Wulashan khondalites: Constraints on the evolution of the Ordos Terrane, Western Block of the North China Craton. Earth and Planetary Science Letters 241, 581–593.

Xiao, L.L., Wu, C.M., Zhao, G.C., Guo, J.H., Ren, L.D., 2011. Metamorphic P–T paths of the Zanhuang amphibolites and metapelites: constraints on the tectonic evolution of the Paleoproterozoic Trans-North China Orogen. International Journal of Earth Sciences 100, 717–739.

Yin, C.Q., Zhao, G.C., Sun, M., Xia, X.P., Wei, C.J., Zhou, X.W., Leung, W.H., 2009. LA-ICP-MS U–Pb zircon ages of the Qianlishan complex: constrains on the evolution of the Khondalite Belt in the Western Block of the North China Craton. Precambrian Research 174, 78–94.

Yin, C.Q., Zhao, G.C., Guo, J.H., Sun, M., Xia, X.P., Zhou, X.W., Liu, C.H., 2011. U–Pb and Hf isotopic study of zircons of the Helanshan Complex: Constrains on the evolution of the Khondalite Belt in the Western Block of the North China Craton. Lithos 122, 25–38.

Zhang, Z.Q., Li, S.M., 1998. Sm–Nd, Rb–Sr age and its geological significance of Archean Taihua Group in Xiongershan, western Henan province. In: Chen, Y.Q. (Ed.), Contributions of Early Precambrian Geology in North China Craton. Geological Publishing House, Beijing, pp. 123–132.

Zhang, G.W., Bai, Y.B., Song, Y., Guo, A.L., Zhou, D.W., Li, T.H., 1985. Composition and evolution of the Archean crust in central Henan, China. Precambrian Research 27, 7–35.

Zhao, G.C., Cawood, P.A., Wilde, S.A., Lu, L.Z., 2000. Metamorphism of basement rocks in the Central Zone of the North China Craton: implications for Paleoproterozoic tectonic evolution. Precambrian Research 103, 55–88.

Zhao, G.C., Wilde, S.A., Cawood, P.A., Sun, M., 2001. Archean blocks and their boundaries in the North China Craton: lithological geochemical, structural and P–T path constraints and tectonic evolution. Precambrian Research 107, 45–73.

Zhao, G.C., Wilde, S.A., Cawood, P.A., Sun, M., 2002. SHRIMP U–Pb zircon ages of the Fuping complex: implications for Late Archean to Paleoproterozoic accretion and assembly of the North China Craton. American Journal of Science 302, 191–226.

Zhao, G.C., Sun, M., Wilde, S.A., 2003. Major tectonic units of the North China Craton and their Paleoproterozoic assembly. Science in China Series D-Earth Sciences 46, 23–38.

Zhao, G.C., Sun, M., Wilde, S.A., Li, S.Z., 2005. Late Archean to Paleoproterozoic evolution of the North China Craton: key issues revisited. Precambrian Research 136, 177–202.

Zhao, G.C., Wilde, S.A., Sun, M., Li, S.Z., Li, X.P., Zhang, J., 2008. SHRIMP U–Pb zircon ages of granitoid rocks in the Lüliang complex: implications for the accretion and evolution of the Trans-North China Orogen. Precambrian Research 160, 213–226.

Zhao, G.C., He, Y.H., Sun, M., 2009. The Xiong'er volcanic belt at the southern margin of the North China Craton: Petrographic and geochemical evidence for its outboard position in the Paleo-Mesoproterozoic Columbia Super continent. Gondwana Research 16, 170–181.